Prototype of a wire-rope rockfall protective fence developed with three-dimensional numerical modeling

著者	Van Phuc Tran, Maegawa Koji, Fukada Saiji
journal or publication title	Computers and Geotechnics
volume	54
page range	84-93
year	2013-10-01
URL	http://hdl.handle.net/2297/39721

doi: 10.1016/j.compgeo.2013.06.008

Prototype of a wire-rope rockfall protective fence developed with three-dimensional numerical modeling

Phuc Tran Van[a,b,*], Koji Maegawa[c], Saiji Fukada[c]

[a]Graduate School of Natural Science and Technology, Kanazawa University, Japan

[b]University of Architecture of Ho Chi Minh City, Vietnam

[c]Department of Environmental Design, Kanazawa University, Japan

[*]Corresponding author. Phuc Tran Van

Graduate School of Natural Science and Technology

Kanazawa University

NST-2C313, Kakuma-machi, Kanazawa, Ishikawa 920-1192, Japan

Tel: +81-76-234-4602, Fax: +81-76-234-4602

E-mail: phucjp@stu.kanazawa-u.ac.jp and phucktruc@gmail.com

Abstract

This study uses a numerical procedure, previously validated with data from full-scale experiments, to investigate the performance of a modified prototype wire-rope fence to provide protection against rockfall. The cost-reducing modifications are increased post spacing and fewer wire netting layers. The numerical procedure provides the nonlinear response of the prototype under various impact conditions and insights into each component's role in dissipating impact energy. A simple but effective method to increase fence capacity is also developed. Finally, the use of two units of the prototype to protect a wide area is investigated employing the numerical procedure.

Keywords: rockfall, numerical procedure, three-dimensional modeling, energy absorber, wire rope, impact location

1. Introduction

In the last 10 years, several models of fences that provide protection from rockfall and have wide-ranging energy absorption capacities have been constructed in areas with steep slopes and/or mountains. Buzzi *et al*. [1] introduced rockfall barriers with a relatively low impact energy absorption capacity of 35 kJ, and Gentilini *et al*. [2-3] reported a series of rockfall protection barriers with energy absorption capacities of 500, 3000, and 5000 kJ.

Ordinarily, the performance of such structures is verified by conducting full-scale tests in which prototypes are subjected to the impact of a block of known mass and velocity [4-7]. However, because of cost and time limitations, full-scale tests cannot be carried out to obtain full knowledge of fence responses under various conditions. Therefore, numerical approaches firmly based on experimental data have been developed that are able to accurately describe the complete response of a fence under dynamic conditions [8-11].

Within this context, we previously developed a new type of rock fence, called the 'wire-rope rockfall protective fence' (abbreviated as WRF) [12]. Two full-scale tests followed by numerical modeling were carried out to thoroughly examine the response of the fence under different impact conditions. Importantly, our numerical approach was thoroughly validated, making it a useful design tool for WRFs. Unfortunately, because of site conditions, the span dimensions (5, 8, and 5 m) of the tested prototype were not fully relevant to practical application. Moreover, wider post spacing would result in appreciable cost benefit because it would reduce post consumption. In this study, we introduce a prototype WRF (referred to hereafter as developed prototype) with a post spacing of up to 10 m in all three modules, as shown in Fig. 1. In addition, our previous work indicated that a second layer of wire netting was largely redundant [12]. Consequently, only one layer of wire netting is used in the newly developed prototype to reduce cost. The effects of these alterations on the response of the fence need to be investigated before

the prototype is used.

In this paper, instead of using an expensive experimental approach, we use our previous numerical procedure [12] to examine the properties of the developed prototype WRF. The elongation, energy absorption capacity, post deformation, and effects of impact location and size of the colliding block are investigated. Particular attention is paid to both the middle and side modules of the developed prototype. Detailed comparison and analysis is used to reveal the performance of the fence under various dynamic conditions and the role of each component of the developed prototype. The performance of the energy absorbers is examined, helping to clarify how the average friction force (abbreviated as AFF; refer to [12] for details) between the wire rope and absorber affects fence elongation, which influences fence efficiency. The findings of this numerical study reveal how to improve fence capacity in a simple and efficient manner. We also consider a practical application in which the site to be protected is wide and requires at least two units of the developed prototype. The performance, particularly the capacity, of a fence composed of two units of the developed prototype is explored. The proposed enhancement method of changing the AFF is verified using iterative numerical models. This is the first time the performance of two units of a rock fence is validated using a numerical procedure, allowing the future practical application of the prototype to be assessed. Furthermore, although the numerical procedure was specifically designed to investigate WRFs, the methodologies and findings derived from this work are likely to help understand the properties of comparable types of rock fence.

A brief description of the developed prototype is given in section 2, and further details are available in Ref. [12]. Section 3 briefly summarizes the numerical procedure and closely scrutinizes the fence response to impacts targeting the middle and side modules. Section 4 proposes an enhancement of the developed prototype and presents interesting ways to improve the fence. Section 5 investigates the practical application of a WRF consisting of two units of

the developed prototype.

2. Description of the developed prototype

The configuration of the developed prototype as depicted in Fig. 1 is the same as that of the previous version of the prototype, except for the post spacing and the number of wire netting layers. The developed prototype WRF has an interception structure, support structure and connecting components (refer to Ref. [12] for additional details). The interception structure is composed of 14 wire ropes, which are primarily responsible for bearing the direct impact of a block, and one layer of wire netting intended to support the wire ropes in arresting the block. The support structure is composed of concrete-filled steel posts, which are rigidly erected on a concrete foundation, and keeps the fence in the vertical plane without requiring lateral cables or anchors. Connecting components include vertical braces, horizontal braces, steel-wire coils, and energy absorbers.

The developed prototype fence has a post spacing of 10 m, nominal height of 4.2 m (defined as the initial vertical distance between the top of the foundation and topmost wire rope), and an interval between wire ropes of 0.3 m.

Figure 2 shows functional details of the energy absorber, which we previously proved both experimentally and numerically to be effective at dissipating impact energy and preventing wire ropes from breaking [12]. The efficiency of the energy absorber is attributed to: (a) the initial motion of the steel block (2) coming into contact with the steel block (1), which prevents a sudden rise in rope tension at the beginning of impact, and (b) the relevant magnitude of the AFF acting between the rope and blocks (1) and (2), which enables the wire rope to slide through the device during the impact. The AFF can be estimated in a laboratory dynamic test [12] and can be altered simply by controlling the torque applied to the bolts connecting the steel

plates in blocks (1) and (2).

3. Numerical analysis of the developed prototype

Although only two features (the post spacing and number of wire netting layers) were altered from our previous WRF [12] to create the developed prototype, we anticipate that these variations will invoke large changes in the structural response of the fence. Expensive experimental approaches have routinely been used to study such prototypes. Here, we employ our previously developed numerical approach [12], which has already been assessed and validated using experimental data obtained in full-scale tests. This inexpensive, accurate approach can precisely produce the nonlinear response of a fence subjected to impacts under dynamic conditions, helping to clarify the capacity of a fence under various impact conditions. In this study, particular attention is paid to the effect of the location of impact on the capacity of the fence along the underlying causes. We also examine the performance of the developed prototype during impact to a side module in terms of fence elongation, end-post response and impact location.

To produce the structural behavior of the fence subjected to the direct impact of a block, numerical simulations are performed with three-dimensional dynamic finite element models using the commercially available computer program LS-DYNA. This explicit program is used to capture dynamic and extremely rapid responses of structures to severe impact loads [9]. The numerical model is primarily based on simplifications of the material properties of fence components, such as the wire ropes (Fig. 3a), wire netting (Fig. 3b), and posts. Figure 4 shows the bending moment *versus* deflection curve of posts obtained from a static laboratory pre-test (refer to Ref. [12] for more details), and an assumed stress-strain curve of the posts. A simplified model of the energy absorbers with AFF=45.4 kN is shown in Figs. 5 and 6. In the numerical

models, the AFF can be easily altered by varying the yield stress. Similarly, to reduce computational cost, the steel coil that connects the wire rope and wire netting, was modeled by a K-element for which the spring constant was 10^5 N/m. The wire netting is a chain-link mesh. The components of the developed prototype, whose numerical parameters are given in Table 1, were assembled in LS-DYNA, as shown in Fig. 7. A cable element with material properties of 'Cable Discrete' that did not consider compressive force was used to model wire rope and wire netting. In addition, a truss element with material properties of 'Piecewise Linear Plasticity', in which a failure strain is adopted, was also used to model the wire rope and netting in the impact section to consider the possibility of the wire breaking.

An automatic-contact based on the penalty method, which involves placing normal interface springs between all penetrating nodes and the contact surface, was used to model the probable interaction between components of the fence.

The colliding block was modeled according to its real shape and its volume was calculated as $V = 17/24 \times L_e^3$ (ETAG-027 2008) [13], where L_e is the maximum size of the block. Elastic-solid elements were assigned to the block with a mass density of 2.63×10^{-9} ton/mm^3. Initially, the trajectory of the colliding block was in a vertical plane perpendicular to the fence plane. The block was assigned initial conditions of angular velocity and translational velocity calculated from a given impact energy.

3.1. Numerical analysis of the functional middle module

This section presents numerical results of simulations of the functional middle module of the developed prototype and discusses the response of the fence under various impact conditions relating to the impact locations shown in Fig. 8 and the size of the colliding block. It is noted that the target impact locations were only at one- and two-thirds of the fence height, which have

been determined as common heights of rockfall impacts in Japan.

Initially, to better understand how the impact location affected the capacity of the fence, we needed to determine the reaction of the fence to impacts of the same energy at different locations. To do this, impacts with an energy of 700 kJ at points A and D in Fig. 8 were examined. The maximum elongation of the fence, deformation of the internal post, and roles played by wire ropes and netting in absorbing impact energy were examined.

Figures 9 and 10 show numerical time histories of fence elongation and deformation of the top of the internal post, respectively, for impacts at points A and D. The differences between the maximum values are as high as 0.45 m for fence elongation and 1.0 m for deformation of the internal post. Therefore, the fence responds differently in the two situations; in the case of an impact at point D, fence elongation depends more on deformation of the internal post than elongation of wire ropes, whereas the opposite is found for an impact at point A. This finding partly reveals the contribution of the internal post to dissipating impact energy through its deformation, especially when the impact location is quite near the internal post.

Figure 11 shows that the tension force of rope 5, which passes through the impact region at two-thirds of the fence height, is slightly higher for an impact at point A than for one at point D. This is opposite to how impact energy is absorbed by the fence components, as shown in Fig. 12. In this case, energy absorbed by the wire ropes and netting is called contact energy, $E_{contact}$, and is incrementally updated from time n to $n + 1$ for each contact interface as [14]:

$$E_{contact}^{n+1} = E_{contact}^{n} + \left[\sum_{i=1}^{nsn} \Delta F_i^{slave} \times \Delta dist_i^{slave} + \sum_{i=1}^{nmn} \Delta F_i^{master} \times \Delta dist_i^{master}\right]^{n+\frac{1}{2}} \quad (1)$$

where nsn is the number of slave nodes, nmn is the number of master nodes, ΔF_i^{slave} is the interface force between the ith slave node and contact segment, ΔF_i^{master} is the interface force between the ith master node and contact segment, $\Delta dist_i^{slave}$ is the incremental distance the ith slave node has moved during the current time step, and $\Delta dist_i^{master}$ is the incremental distance the ith master node has moved during the current time step.

Figure 12 shows that the wire ropes absorbed less energy for an impact at point D than at point A. Point A is further from the internal post, so impact momentum is therefore transferred over a longer distance from the impact region to the post and dissipated more by rope elongation (known as strain energy), resulting in more severe conditions for the wire ropes. In addition, as shown in Fig. 12a, the portion of impact energy absorbed by the wire ropes is greater for an impact at point A than at D, whereas the kinetic energy absorbed by the internal post is zero. The situation for an impact at point D is the opposite, as shown in Fig. 12b. The sizable deformation of the internal post in this case illustrates the post absorbs more impact energy, and this appears to be a consequence of a large proportion of the impact momentum being transferred by the wire ropes over a shorter distance. Figure 12b also reveals that the total impact energy absorbed by the wire ropes and netting is less than 700 kJ, which is the initial impact energy imparted by the colliding block. This means that a small proportion of the impact energy (30 kJ) is absorbed by the deformation of the internal post. Figure 13 shows that for an impact at point D, the fence arrests the block a little quicker than at point A, again suggesting that the internal post absorbs appreciable energy through its large deformation.

We performed iterative calculations to examine the effects of impact location and the size of the colliding block on the capacity of the fence. Impact locations were at one- and/or two-thirds of the fence height. For impacts at one-third height, fewer impact locations and block sizes needed to be investigated, and the translational velocity component of the block in the Z direction was eliminated to prevent the block from landing on the ground during impact. The Rockfall Mitigation Handbook [15] recommends that the rotational energy is consistently set as high as 10% of the total impact energy in all cases and the maximum translational velocity of the colliding block should be around 30 m/s. The minimum size of the block was therefore set as 1000 mm, because if the block was smaller than this, the magnitude of the translational velocity was certain to exceed the limitation of 30 m/s. Thus, three blocks with maximum size L_e of

1000, 1200, and 1400 mm were chosen as typical colliding rock blocks. Table 2 presents numerical results derived from the survey that are relevant to the maximum energy absorption of the fence (*i.e.*, the highest kinetic energy of a block that can be stopped by the fence) under various conditions of impact location and block size.

For all dimensions of the block, the fence capacity gradually increases along the line of impact points from A through D; *i.e.*, the capacity of the fence is highest for an impact at point D. This trend is unaffected by block size, and the nearer the impact is to the internal post, the higher the capacity of the fence. This is inconsistent with results reported by Cazzani *et al*. [8]; the reason for this discrepancy is the different design of the two fences in terms of stiffness. Table 2 also shows that the fence capacity depends on the size of the block, gradually weakening as the block size decreases. This result is consistent with those of Cazzani *et al*. [8], Spadari *et al.* [16], and Hambleton *et al*. [17]. This relation can be simply explained by the fact that for the same impact energy, the smaller the block, and the greater its velocity, especially its rotational velocity component. This facilitates the block rolling over the fence when the impact is targeted at two-thirds of the fence height. An exception is point E, where no dependence on block size is observed. This is because elongation of the wire ropes dominates, which leads to large deformation of the fence so the block easily rolls through the bottom of the fence without rope breakage. In addition, it is likely that the decrease in fence capacity caused by the small deformation of the internal post. The above findings suggest that the block size should be considered seriously when determining fence capacity.

Interestingly, we observed that in almost all cases of the fence failing to catch the block because impact energy exceeds fence capacity, the block rolls over or under the fence without any breakage of wire ropes, which is attributed to critical elongation of the fence (the maximum elongation at which the fence can catch the block). This means that critical elongation is a factor that can be optimized to enhance the performance of the fence. Specifically, the critical

elongation should be high enough to entirely absorb kinetic energy and catch the block, but not so high that it allows the block to roll over the fence.

3.2. Numerical analysis of the functional side module

This section explores the performance of the fence with impacts on the side module. Similar to the analysis of the middle module, the response of the fence to impacts with an energy of 700 kJ at points H and I indicated in Fig. 14 was investigated in terms of fence elongation, displacement of the top of the end post, bending moment acting on the base of the end post, impact energy absorbed by the wire ropes and netting, and velocity of the block.

Figure 15 shows the numerical time histories of the fence elongation for impacts at points H and I. The difference in peak values of 0.4 m is approximately the same as that in the case of the middle module (0.45 m; Fig. 9). However, the trends of the fence elongation history are different for the two cases examined for the side module, particularly at the beginning of impact. This is explained by the greater effect of energy absorbers, which are immediately next to the impact location, on the fence response to an impact at point I than at H. In other words, after much sliding of the wire ropes through the absorbers resulting in larger elongation of the fence at the beginning of impact, the stoppers hit the absorbers and slow the lengthening of the wire ropes, causing the fence elongation to become less severe (Fig. 15). Another reason is the difference in the deformation of the end post between the two cases, as depicted in Fig. 16. Figure 16 illustrates the displacements of the top of the end post in both X and Y directions for impacts at points H and I. For impacts at both points, the end post deformation is relatively similar in the X and Y directions. Deformation increased as the peak values exceed 1.5 m, resulting in a critical moment (over 700 kNm) measured at the base of the end post, as shown in Fig. 17.

Figure 18 shows that although the proportions of impact energy absorbed by the wire ropes and netting vary in the two cases, the total absorbed energy is slightly less than the initial impact energy of 700 kJ, and similar to the energy absorbed during the impact at point D of the middle module. These results further confirm the contribution from the deformation of posts to dissipating energy.

Comparison of Fig. 13 and 19 reveals that the fence takes longer to catch the block in the case of an impact on the side module than the middle one. In addition, compared with impacts at points A and D of the middle module, the difference of the general response of the fence between impacts at points H and I is small. This is further evidenced by numerical results obtained for a series of simulations investigating fence capacity for various impact locations, as shown in Table 3. Indeed, the fence capacity remains unchanged at 700 kJ for impacts at points H, I, K, and L, and the capacity of the side module is less than that of the middle one. This is attributed to the large deformation of the end post, especially in the X direction. For an impact energy of 800 kJ targeted at point H, the end post breaks at its base, as depicted in Fig. 20 and the block rolls over the fence. The post breaks in this case because the effective plastic strain at its base exceeds the critical magnitude of 0.35 as a failure condition, which is the average value of effective plastic strain Ip1–Ip4 (Ip1–Ip4 are four integral points of a beam element). Effective plastic strain can be calculated as [14]:

$$\varepsilon_p = \varepsilon - \left(\frac{\sigma}{E}\right), \tag{2}$$

where ε is total strain, σ is true stress, and E is Young's modulus.

When the impact energy is reduced to 750 kJ, the end post does not break but the fence does not stop the block. However, the fence exhibits higher strength for impacts at points G and J, which are quite far from the end post. The fence response in these cases is not dominated by large deformation of the end post. Like points D and F, points G and J are located next to the internal post. Therefore, the fence response can be explained by the contribution of the internal post to

dissipating impact energy, as discussed in section 3.1.

4. Improvement of the developed prototype

For impacts at two-thirds of the fence height, the fence fails to catch the block because it rolls over the top of the fence. This is because the residual height of the fence is reduced considerably through its large elongation. Therefore, lessening fence elongation is important to enhance its effectiveness. In an effort to reduce the elongation of the fence, numerical simulations of an impact at point A of the middle module with impact energy of 800 kJ and various AFFs of the absorber were carried out to explore the relationship between fence elongation and AFF.

Figure 21 reveals that fence elongation is independent of the AFF at the beginning of impact; *i.e.*, the absorbers have not yet come into effect. Initially, fence elongation is attributed to elongation of the wire ropes and deformation of the post. When the absorbers start to take effect, the fence elongation decreases slightly as the AFF increases from 50 to 60 kN. However, surprisingly, fence elongation remains unchanged as the AFF increases from 60 to 70 kN. It is likely that at an energy of 800 kJ, AFF=60 kN is a threshold at which the absorbers still affect fence elongation. Moreover, according to a preliminary test of the energy absorbers, the maximum friction force acting between the wire rope and absorber is probably three times the AFF [12]. Therefore, AFF=70 kN is inappropriate because the critical strength of the wire ropes is 180 kN. Overall, AFF=60 kN both reduces fence elongation and prevents the wire ropes from breaking. For AFF=60 kN, the fence capacity for an impact at point A of the middle module increases to 950 kJ from the original value of 800 kJ corresponding to AFF=45 kN, which is an increase of 19% (Fig. 22).

More interestingly, the numerical results in Fig. 23 show that the energy absorption capacity of the fence for an impact at point E of the middle module increases from 400 kJ for AFF=45 kN to 750 kJ for AFF=60 kN, which is an increase of 87%. This improvement is considerable, and

suggests that the fence capacity is especially sensitive to the elongation of the wire ropes in this case.

These results show that the developed prototype fence can be strengthened considerably by optimizing the AFF simply by altering the torque of the M20 bolts [12]. The fence becomes more effective as it is made stiffer, which is unusual for flexible fences. However, it seems logical in this case because the failure mechanism is the block rolling over the fence rather than its breakage.

5. Practical application of the developed prototype

In practice, the length of a site that needs to be protected commonly exceeds the prototype length (30 m). In this case, at least two units of the developed prototype must be erected side by side, as shown in Fig. 24, where two units are joined by a connecting post. The performance of the fence as a whole against impacts on modules M1 and M2 is expected to differ from that of an individual unit because the response of the connecting post (regarded as the end post in a single unit) is influenced by the second unit; it is thus important to investigate this scenario.

To carry out this analysis, iterative numerical models were calculated. Results for the energy absorption capacity of modules M1 and M2 as constituents of the whole fence are presented in Table 4. For brevity, only two impact locations are considered for each module, one at one-third height (points N and W) and the other at two-thirds height (points M and O) of the fence at the center of the horizontal span, as indicated in Fig. 24. Specifically, points M, O, N, and W in Fig. 24 correspond to points A, I, E, and L, respectively, in Figs. 8 and 14.

The numerical data summarized in Table 4 show a sizable increase in the fence capacity when two units are placed side by side. Specifically, the increases in fence capacity are approximately 37% and 36% for impacts at points M and O, respectively, with respect to the capacity of a

single unit. The corresponding increases for impacts at points N and W are 25% and 21%, respectively. Indeed, the improvement of the fence performance in this situation is even greater than that in the case of optimizing the AFF as discussed above. This can be attributed to the reduced deformation of the connecting post because it is constrained by the second unit, resulting in a large decrease in overall fence elongation, as seen by comparing Fig. 25 with Figs. 9 and 15.

Next, the enhancement approach of altering the AFF (from 45 to 60 kN) was applied to the joined fence units. The fence capacity increases considerably, as expected. The energy absorption capacity of the fence increases to 1200 and 750 kJ for impacts at points M and N, respectively. Similar to the case of one unit, the increase of fence capacity for an impact at point N is larger than that for an impact at point M when the AFF is changed.

6. Conclusions

On the basis of our previous work [12], we developed a new prototype WRF mainly for cost reasons. The prototype was investigated using a numerical procedure we previously validated with experimental data obtained in full-scale tests. In this study, we examined the nonlinear responses of functional middle and side modules of the developed prototype to the impact of a block with varying mass and velocity. Our results provided insight into how the fence reacts to impacts under different conditions, revealing the role of each component. Of particular interest was the contribution of posts to dissipating energy.

From the knowledge obtained about this prototype and its capacity limitations, an approach to improve fence performance was suggested. Simply optimizing the AFF of the energy absorbers was numerically demonstrated to improve fence performance. The energy absorption capacity of the fence increased by at least ~20% (150 kJ), matching the capacity of other types of rock

fence [12]. The AFF can be changed simply by controlling the torque of the M20 bolts connecting the components of the energy absorber.

We also considered the common situation in which a fence composed of two units of the prototype was used to protect a wide area. Employing the same numerical procedure used earlier in the study, we analyzed iterative models to clarify the performance of the longer fence. The longer fence was also strengthened by optimizing the AFF, confirming the effectiveness of this approach for the developed prototype. Although the response of the developed prototype was only analyzed by a numerical approach, the results obtained are valuable for the practical application of this prototype, and for further research on this or similar types of rock fence.

Acknowledgements

The authors wish to thank Raiteku Company, Japan for the great support and Mr. Trung and Mr. Son for high-quality drawings. Special thanks are also due to two anonymous reviewers who very minutely commented over the manuscript, thereby helping to improve it to the present stage. Last but not least, the first author is thankful to his wife Tran Thao Nhi for her assistance throughout.

References

[1] Buzzi O, Spadari M, Giacomini A, Fityus S, and Sloan SW. Experimental Testing of Rockfall Barriers Designed for the Low Range of Impact Energy. J Rock Mechanics and Rock Engineering, 2012.

[2] Gentilini C, Gottardi G, Govoni L, Mentani A, and Ubertini F. Design of falling rock protection barriers using numerical models. J Engineering structures, 2013; 50:96-106.

[3] Gentilini C, Govoni L, de Miranda S, Gottardi G, and Ubertini F. Three-dimensional numerical modelling of falling rock protection barriers. J Computers and Geotechnics, 2012;

44:58–72.

[4] Gottardi G and Govoni L. Full-scale Modelling of Falling Rock Protection Barriers. J Rock Mechanics and Rock Engineering, 2009; 43:261–274.

[5] Peila D, Pelizza S, and Sassudelli F. Evaluation of Behaviour of Rockfall Restraining Nets by Full Scale Tests. J Rock Mechanics and Rock Engineering, 1998; 31:1–24.

[6] Tajima T and Maegawa K. Evaluation of Pocket-type Rock Net by Full Scale Tests. IABSE, 2009.

[7] Arndt B, Ortyz T, and Turner AK. Colorado ' s Full-Scale Field Testing of Rockfall Attenuator Systems. Transportation research board of the national academies, 2009.

[8] Cazzani A, Mongiovì L, and Frenez T. Dynamic finite element analysis of interceptive devices for falling rocks. J Rock Mechanics and Mining Sciences, 2002; 39:303–321.

[9] Dhakal S, Bhandary NP, Yatabe R, and Kinoshita N. Experimental, numerical and analytical modelling of a newly developed rockfall protective cable-net structure. J Natural Hazards and Earth System Science, 2011; 11:3197–3212.

[10] Volkwein A. Numerical Simulation of Flexible Rockfall Protection Systems. J Computing in Civil Engineering, 2005; 179:122–122.

[11] Sasiharan N, Muhunthan B, Badger T, Shu S, and Carradine D. Numerical analysis of the performance of wire mesh and cable net rockfall protection systems. J Engineering Geology, 2006; 88:121–132.

[12] Tran PV, Maegawa K, and Fukada S. Experiments and Dynamic Finite Element Analysis of a Wire-Rope Rockfall Protective Fence. J Rock Mechanics and Rock Engineering, 2012.

[13] ETAG-027 (2008) Guideline for European Technical Approval of Falling Rock Protection Kits. European Organization for Technical Approvals (EOTA)

[14] Hallquist JO. LS-DYNA Theory Manual. Livermore Software Technology Corporation,

2006.

[15] Japan Road Association. Rockfall Mitigation Handbook, 2006.

[16] Spadari M, Giacomini A, Buzzi O, and Hambleton J P. Prediction of the bullet effect for rockfall barriers: a scaling approach. J Rock Mechanics and Rock Engineering, 2012; 45: 131-144.

[17] Hambleton J P, Buzzi O, Giacomini A, and Sloan S W. Perforation of flexible rockfall barriers by normal block impact. J Rock Mechanics and Rock Engineering, 2013; 46: 515-526.

[18] Dhakal S, Bhandary NP, Yatabe R, and Kinoshita N. Numerical and analytical investigation towards performance enhancement of a newly developed rockfall protective cable-net structure. J Natural Hazards and Earth System Science, 2012; 12: 1135–1149.

Caption for figures

Fig. 1. Schematic drawing of the developed prototype.

Fig. 2. Energy absorbing device.

Fig. 3. Assumed stress–strain curve applied for wire ropes (a) and wire netting (b)

Fig. 4. Bending moment vs. deflection curve of posts (a) and assumed stress–strain curve of posts (b)

Fig. 5. Numerical model applied for energy absorber

Fig. 6. Simplification assumption of energy absorbers.

Fig. 7. Technical sketch of the developed prototype built in LS-DYNA.

Fig. 8. Map of impacts on the middle module.

Fig. 9. Numerical time histories of fence elongation for impacts at points A and D.

Fig. 10. Numerical time histories of the deformation of the top of the internal post for impacts at points A and D.

Fig. 11. Numerical time histories of tension force of rope No. 5 for impacts at points A and D.

Table 1
Numerical data for the fence modelled in LS-DYNA.

Structural Component	Type of Element	Type of Material	Sectional Properties [mm]
Wire rope	a) Beam-Cable b) Beam-Truss	a) Cable Discrete b) Piecewise Linear Plasticity– Failure strain of 0.06	∅18
Wire netting	a) Beam-Cable b) Beam-Truss	a) Cable Discrete b) Piecewise Linear Plasticity– Failure strain of 0.4	∅5
Post	Beam	Piecewise Linear Plasticity – Failure strain of 0.35	∅267.4 × 30t
Horizontal Brace	Beam	Piecewise Linear Plasticity – Failure strain of 0.35	∅14.3 × 4.5t
Vertical Brace	Shell	Piecewise Linear Plasticity – Failure strain of 0.35	9t
Steel ring welded to post	Beam	Rigid	∅30
U-bolts connected to vertical brace	Beam	Rigid	∅10

Table 2
Numerical results for fence capacity at different impact locations (points A–F of the middle module) and various block sizes. L_e: maximum size of block; Critical E: highest kinetic energy of a block that can be stopped by the fence.

Points	L_e = 1000 mm		L_e = 1200 mm		L_e = 1400 mm	
	Critical E (kJ)	v_y (m/s)	Critical E (kJ)	v_y (m/s)	Critical E (kJ)	v_y (m/s)
Point A	700	25.9	720	19.9	800	16.5
Point B	720	26.3	750	20.3	820	16.7
Point C	750	26.8	850	21.6	950	18.0
Point D	950	30.9	970	23.1	1100	18.9
Point E	400	19.7	400	14.9	400	11.6
Point F	800	27.8	900	22.4	1000	18.6

Table 3
Numerical results for fence capacity at different impact locations of the side module.

Point	H	I	K	L	G	J
Critical E (kJ)	700	700	700	700	850	1200
v_y (m/s)	15.4	15.4	15.4	15.4	17.0	20.3
Failure mechanisms	Rolling over	Rolling over	Perforation with rope breaking	Perforation with rope breaking	Rolling over	Perforation with rope breaking

Table 4
Energy absorption capacity of a fence composed of two units of the developed prototype.

	Module M1			Module M2
Point	Critical E (kJ)		Point	Critical E
	AFF=45 kN	AFF=60 kN		(kJ)
M	1100	1200	O	950
N	500	750	W	850

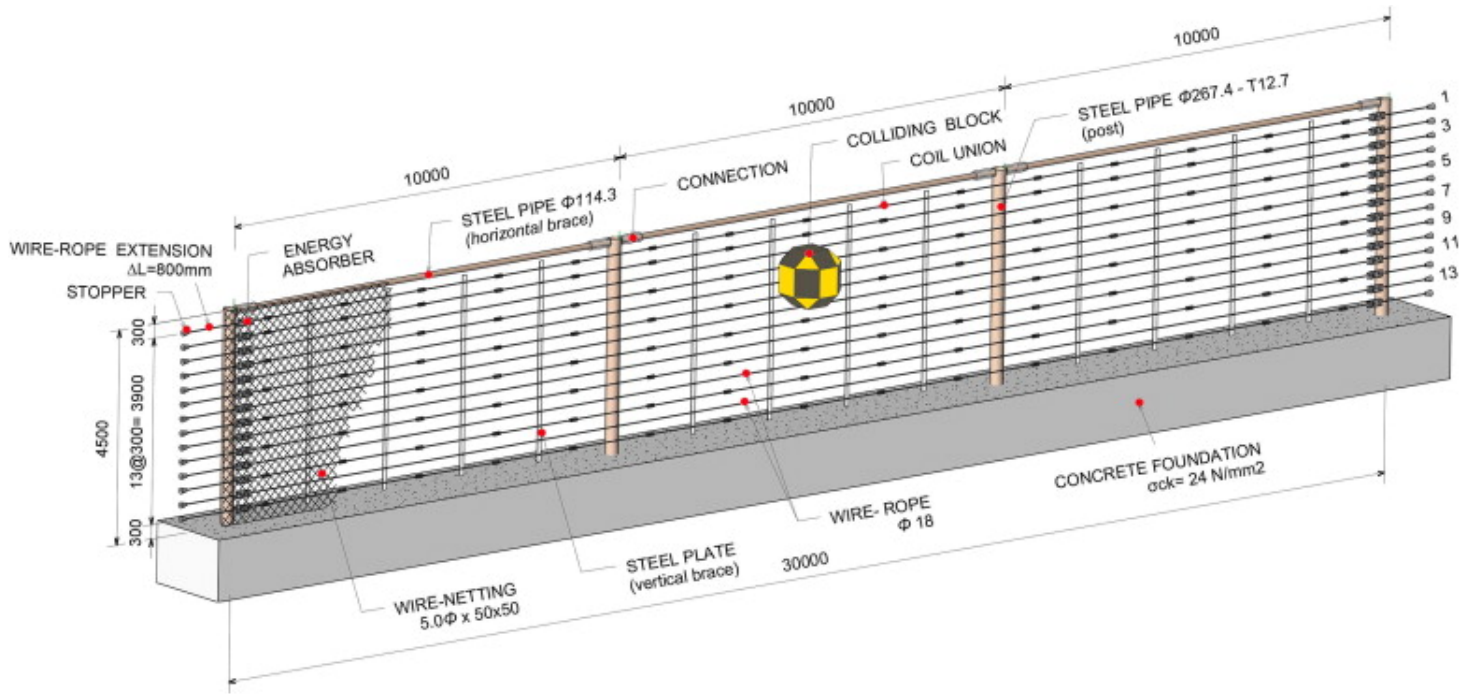
10000
10000
10000
WIRE-ROPE EXTENSION
ΔL=800mm
STOPPER
ENERGY ABSORBER
STEEL PIPE Φ114.3
(horizontal brace)
CONNECTION
COLLIDING BLOCK
COIL UNION
STEEL PIPE Φ267.4 - T12.7
(post)
1
3
5
7
9
11
13
4500
300
13@300= 3900
300
WIRE-NETTING
5.0Φ x 50x50
STEEL PLATE
(vertical brace)
30000
WIRE- ROPE
Φ 18
CONCRETE FOUNDATION
σck= 24 N/mm2

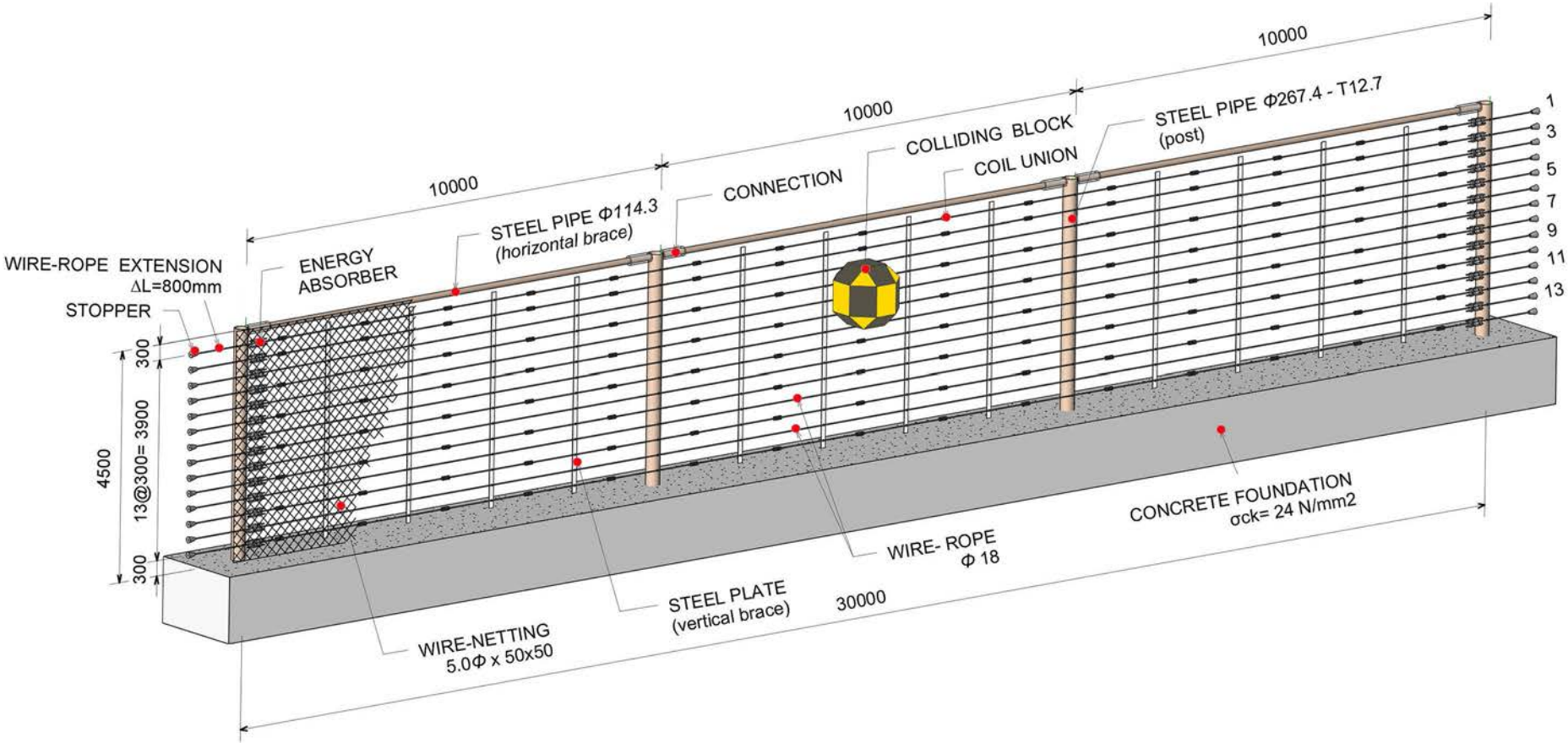
10000
10000
10000
WIRE-ROPE EXTENSION
ΔL=800mm
STOPPER
ENERGY
ABSORBER
STEEL PIPE Φ114.3
(horizontal brace)
CONNECTION
COLLIDING BLOCK
COIL UNION
STEEL PIPE Φ267.4 - T12.7
(post)
1
3
5
7
9
11
13
300
13@300= 3900
300
4500
WIRE-NETTING
5.0Φ x 50x50
STEEL PLATE
(vertical brace)
30000
WIRE- ROPE
Φ 18
CONCRETE FOUNDATION
σck= 24 N/mm2

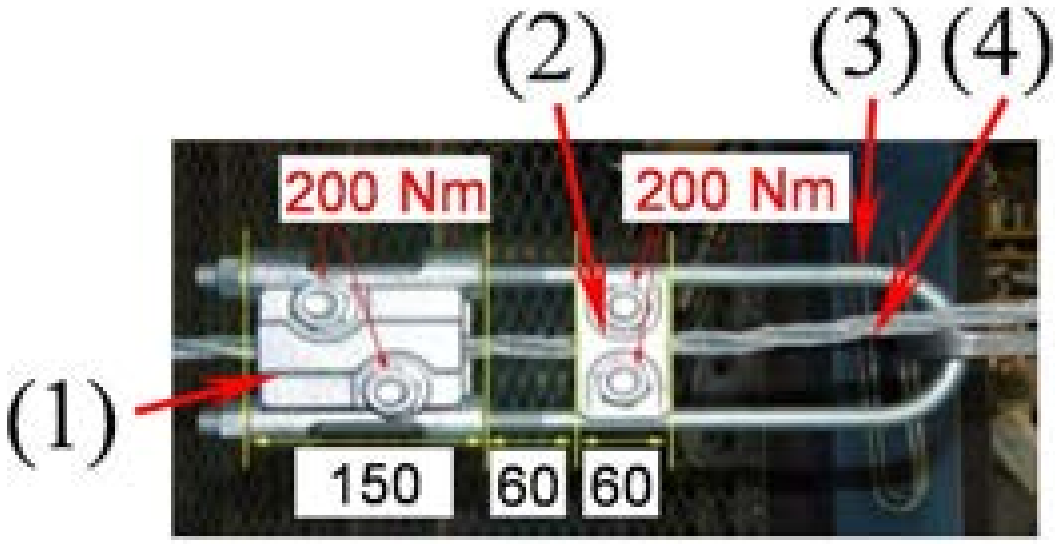

(1) is fixed to (3)-(2) can initially move along (3)-(4) can slip through (1) & (2).

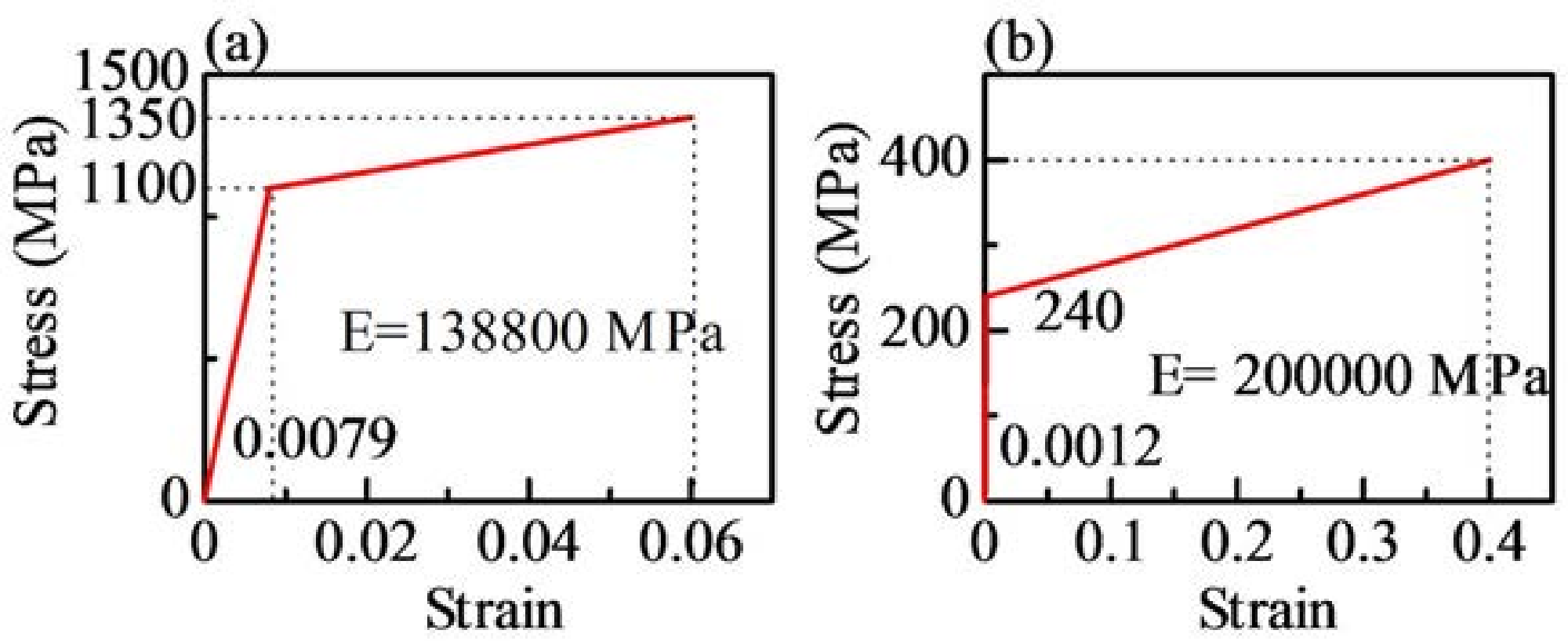
(a)
1500
1350
1100
0
Stress (MPa)
E=138800 MPa
0.0079
0
0.02
0.04
0.06
Strain
(b)
400
200
0
Stress (MPa)
240
E= 200000 MPa
0.0012
0
0.1
0.2
0.3
0.4
Strain

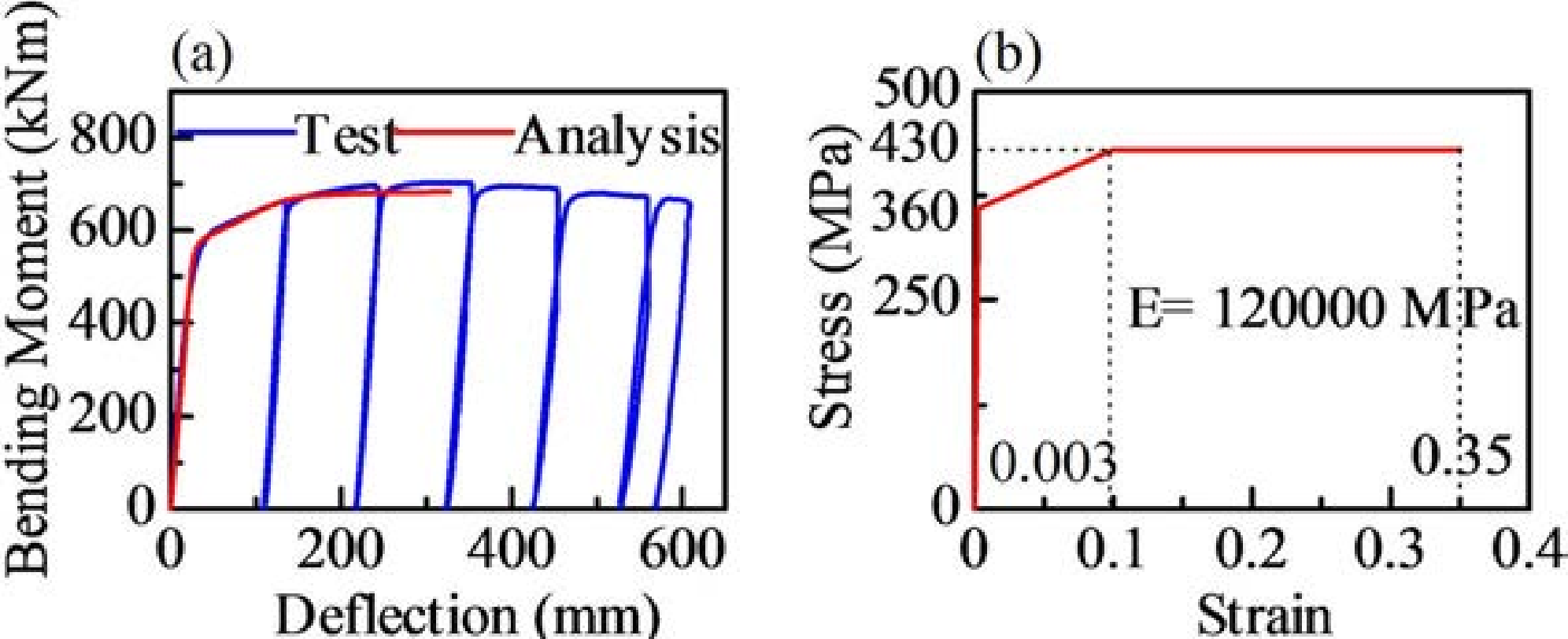
(a)
Test
Analysis
Bending Moment (kNm)
800
600
400
200
0
0
200
400
600
Deflection (mm)
(b)
500
430
360
250
0
Stress (MPa)
E= 120000 MPa
0.003
0.35
0
0.1
0.2
0.3
0.4
Strain

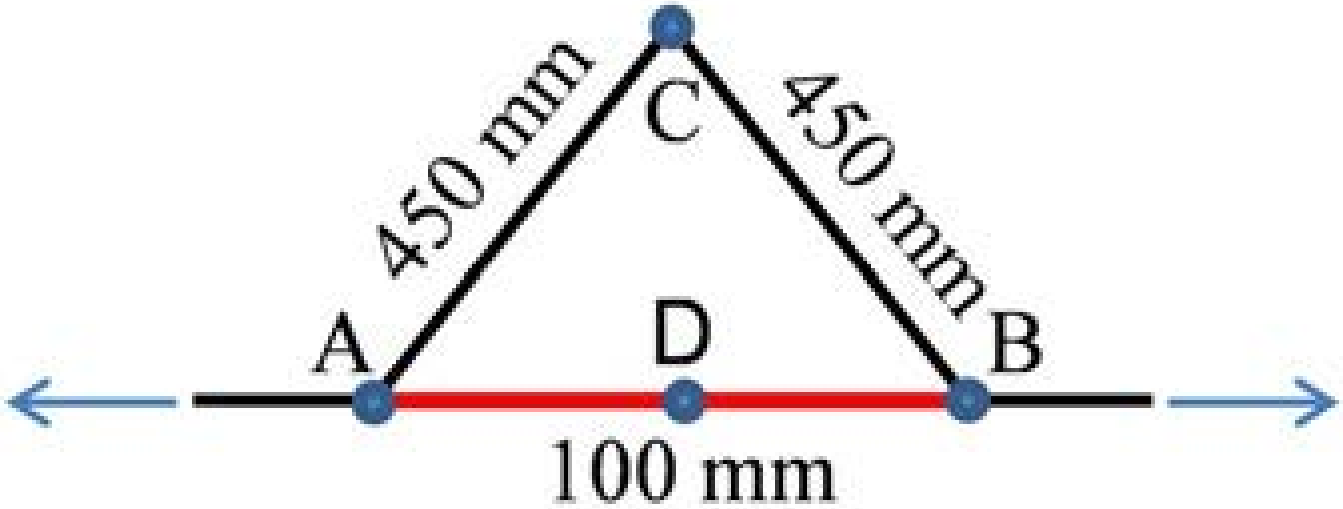
450 mm
C
450 mm
A
D
B
100 mm

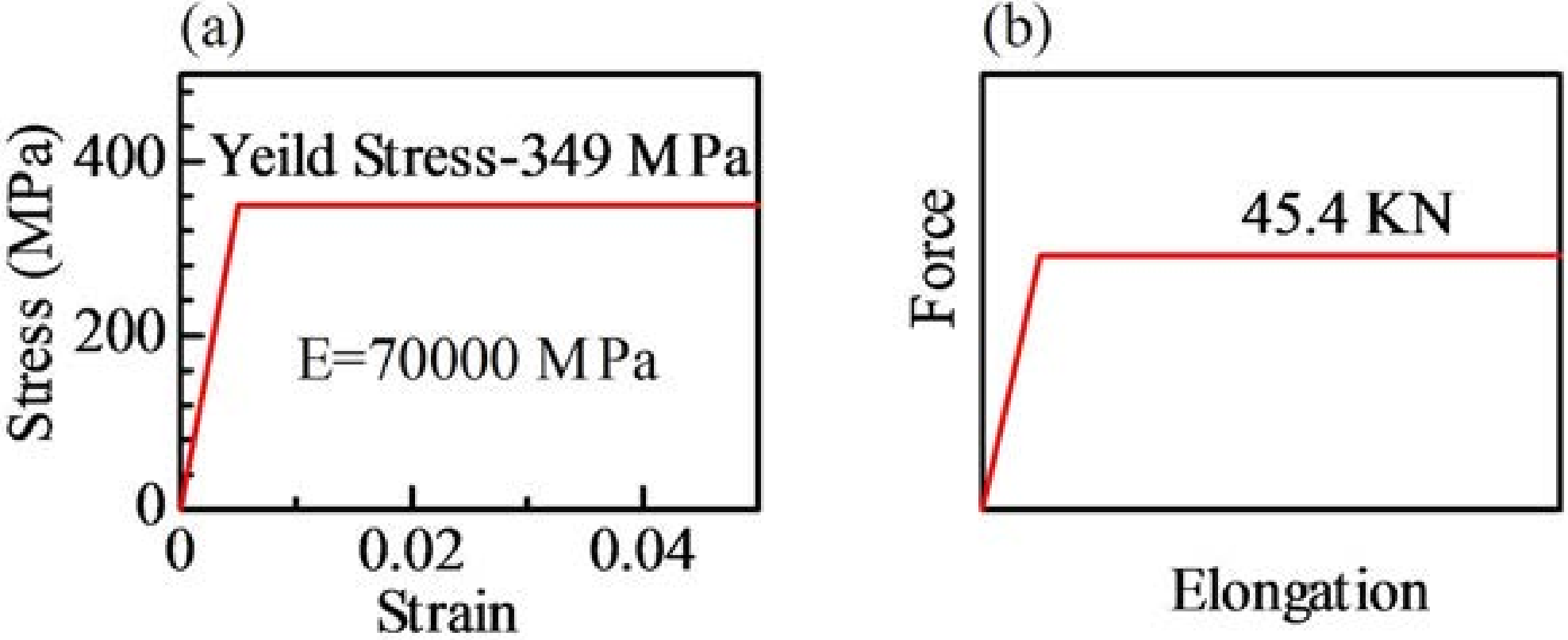
(a)
Stress (MPa)
400
200
0
Yeild Stress-349 MPa
E=70000 MPa
0
0.02
0.04
Strain
(b)
Force
45.4 KN
Elongation

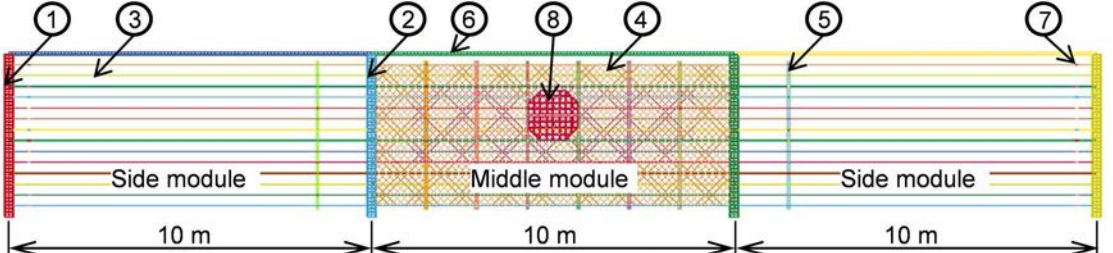
①
③
②
⑥
⑧
④
⑤
⑦
Side module
Middle module
Side module
10 m
10 m
10 m
Z
Y
X
① End post
② Intermediate post
③ Wire rope
④ Wire netting
⑤ Vertical brace
⑥ Horizontal brace
⑦ Energy absorber
⑧ Colliding block

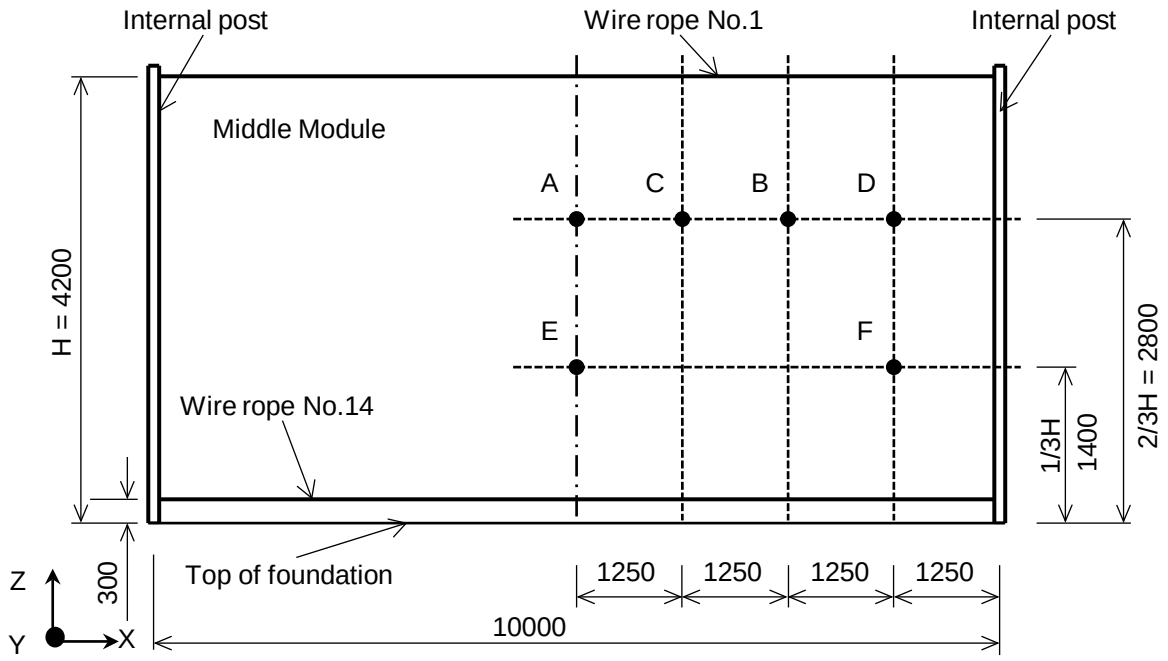
Internal post
Wire rope No.1
Internal post
Middle Module
A
C
B
D
E
F
H = 4200
Wire rope No.14
1/3H
1400
2/3H = 2800
Top of foundation
300
Z
Y
X
1250
1250
1250
1250
10000

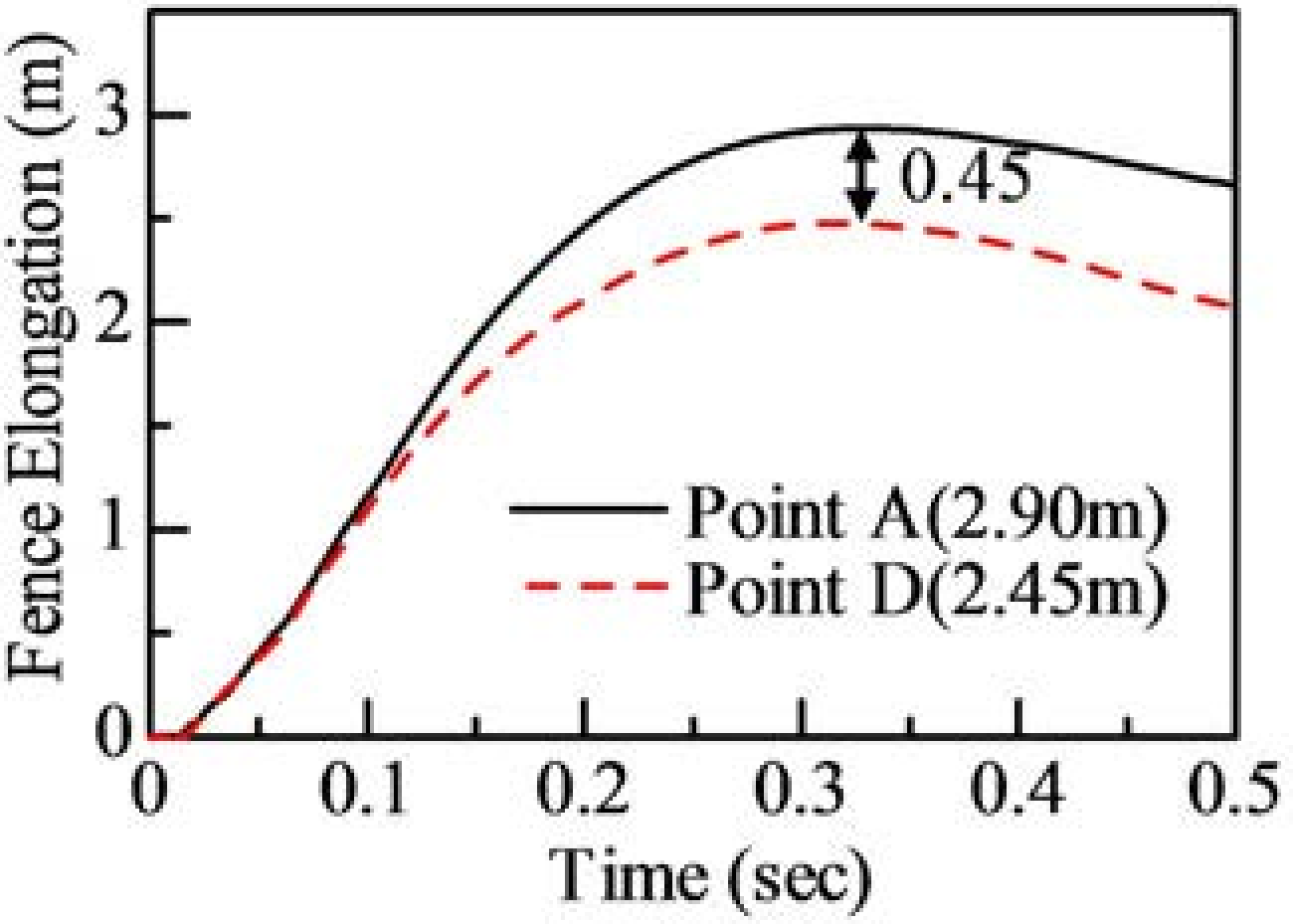
Fence Elongation (m)
3
2
1
0
0.45
Point A(2.90m)
Point D(2.45m)
0
0.1
0.2
0.3
0.4
0.5
Time (sec)

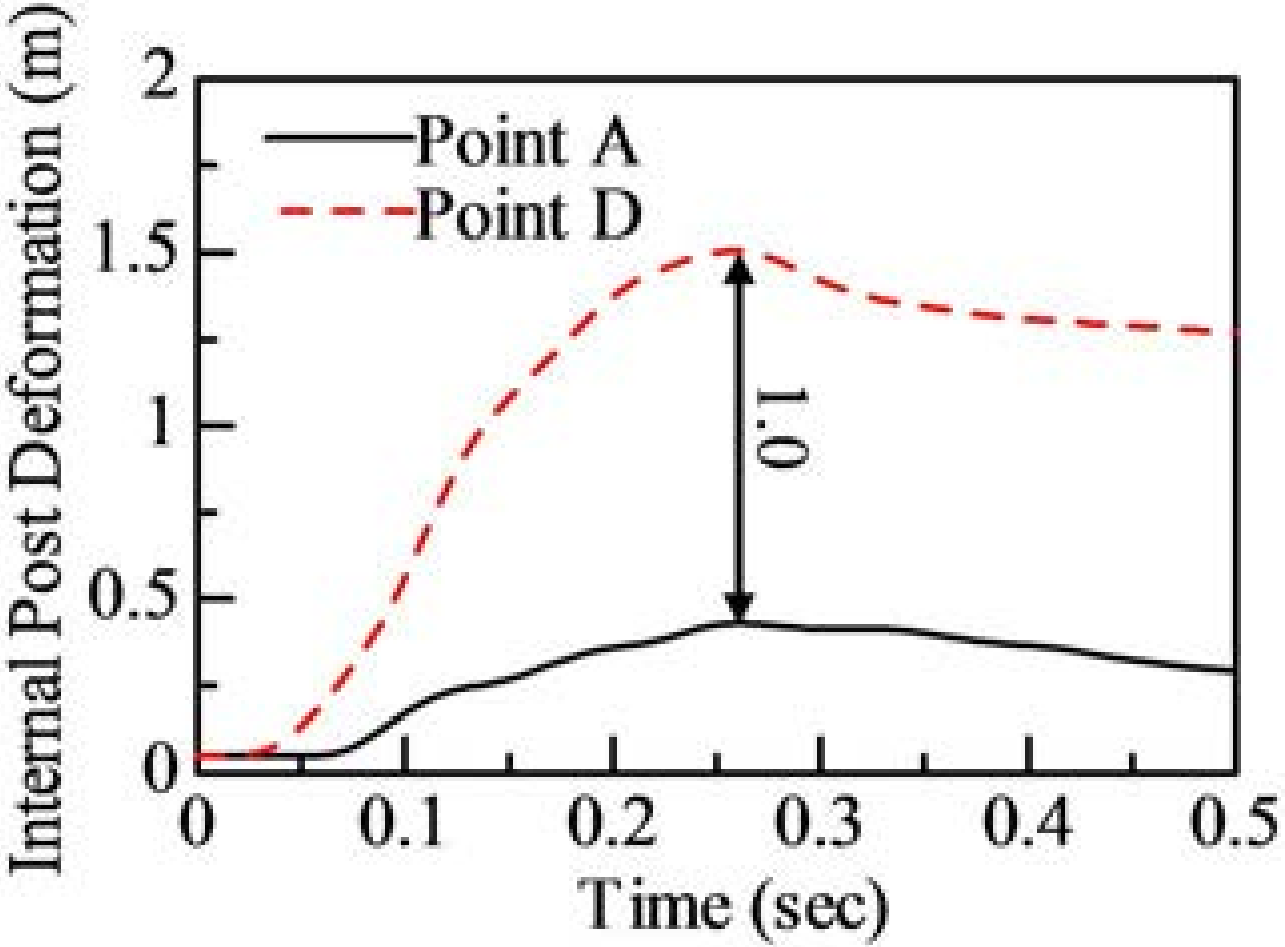
Point A
Point D
1.0
Internal Post Deformation (m)
Time (sec)
0
0.5
1
1.5
2
0
0.1
0.2
0.3
0.4
0.5

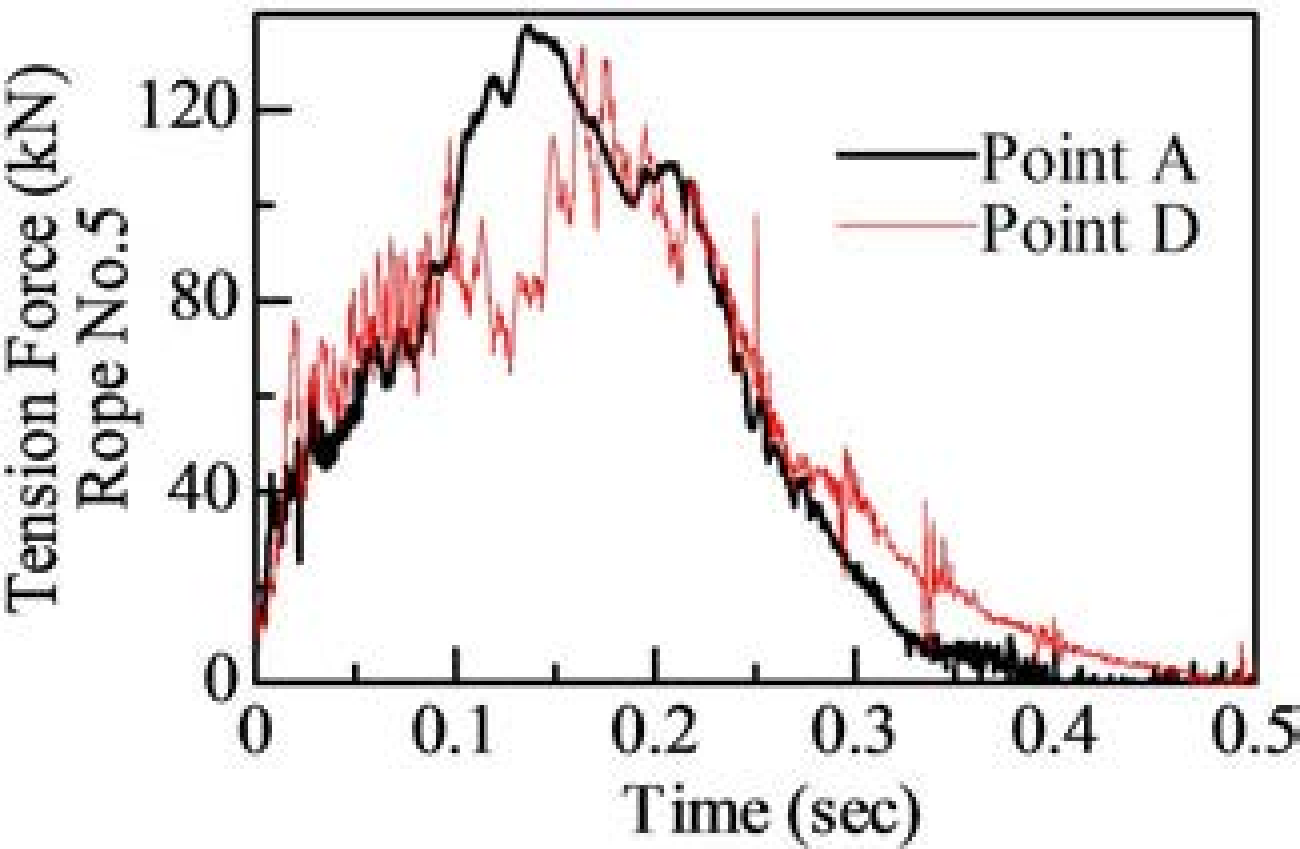
Tension Force (kN)
Rope No.5
120
80
40
0
0
0.1
0.2
0.3
0.4
0.5
Time (sec)
Point A
Point D

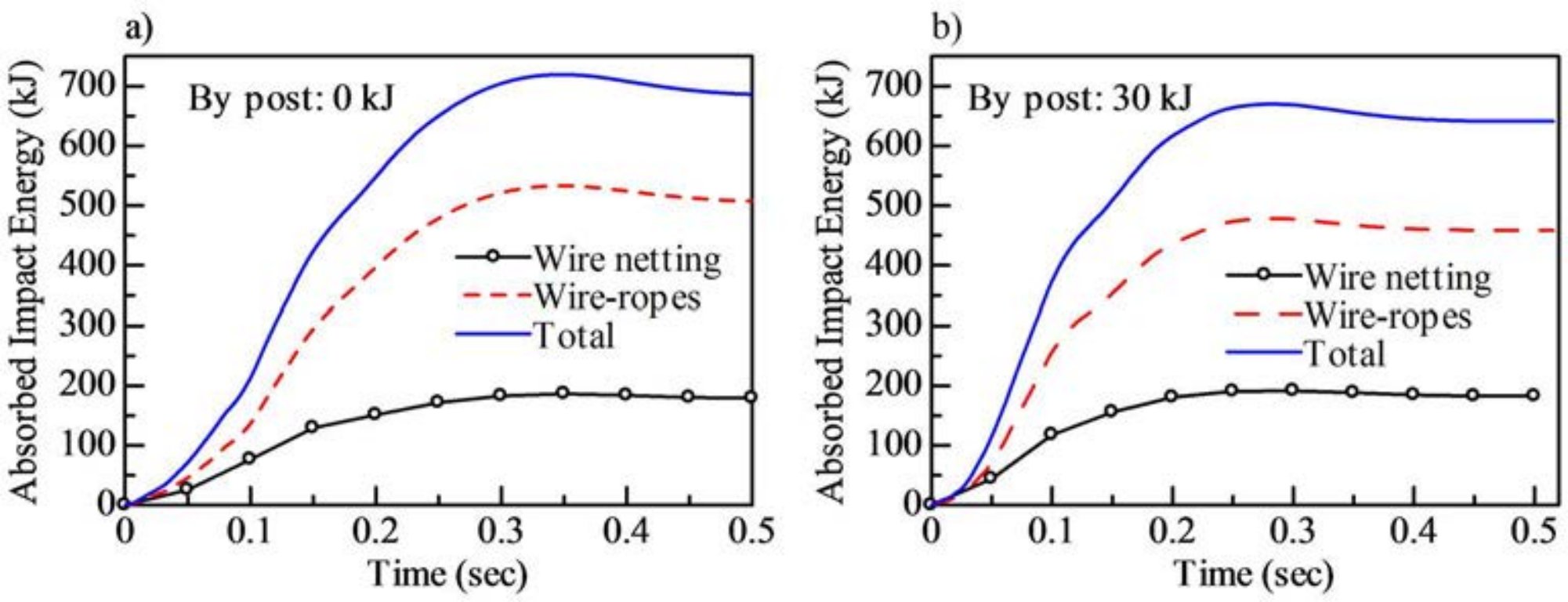
a)
By post: 0 kJ
Absorbed Impact Energy (kJ)
Time (sec)
Wire netting
Wire-ropes
Total
b)
By post: 30 kJ
Absorbed Impact Energy (kJ)
Time (sec)
Wire netting
Wire-ropes
Total

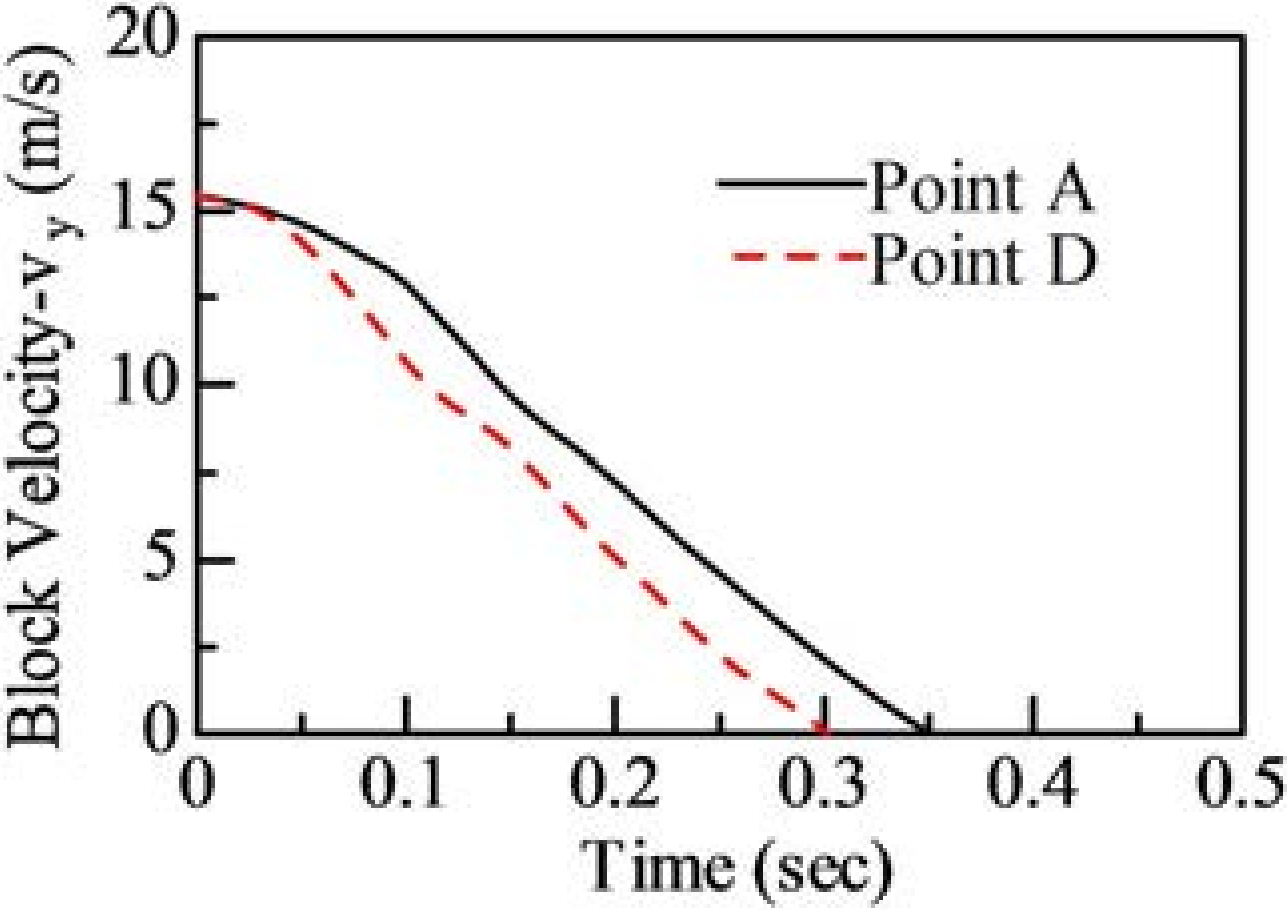
Block Velocity-v_y (m/s)
20
15
10
5
0
0
0.1
0.2
0.3
0.4
0.5
Time (sec)
Point A
Point D

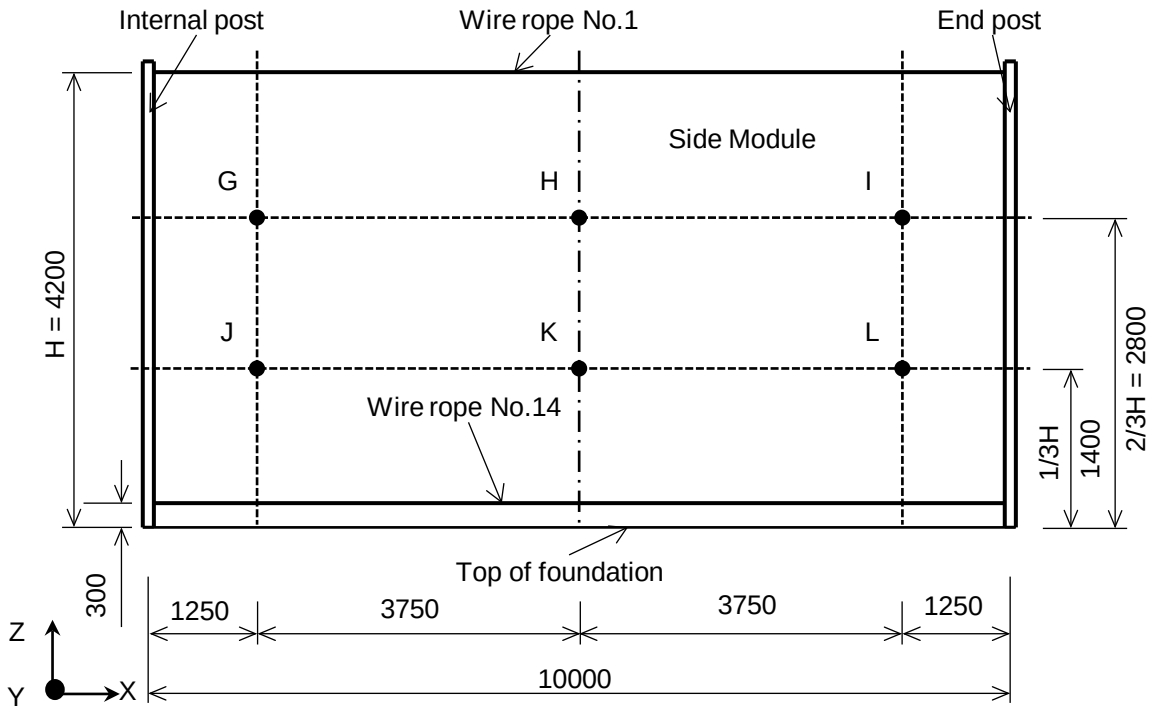
Internal post
Wire rope No.1
End post
Side Module
G
H
I
J
K
L
H = 4200
2/3H = 2800
1/3H
1400
Wire rope No.14
Top of foundation
300
1250
3750
3750
1250
10000
Z
Y
X

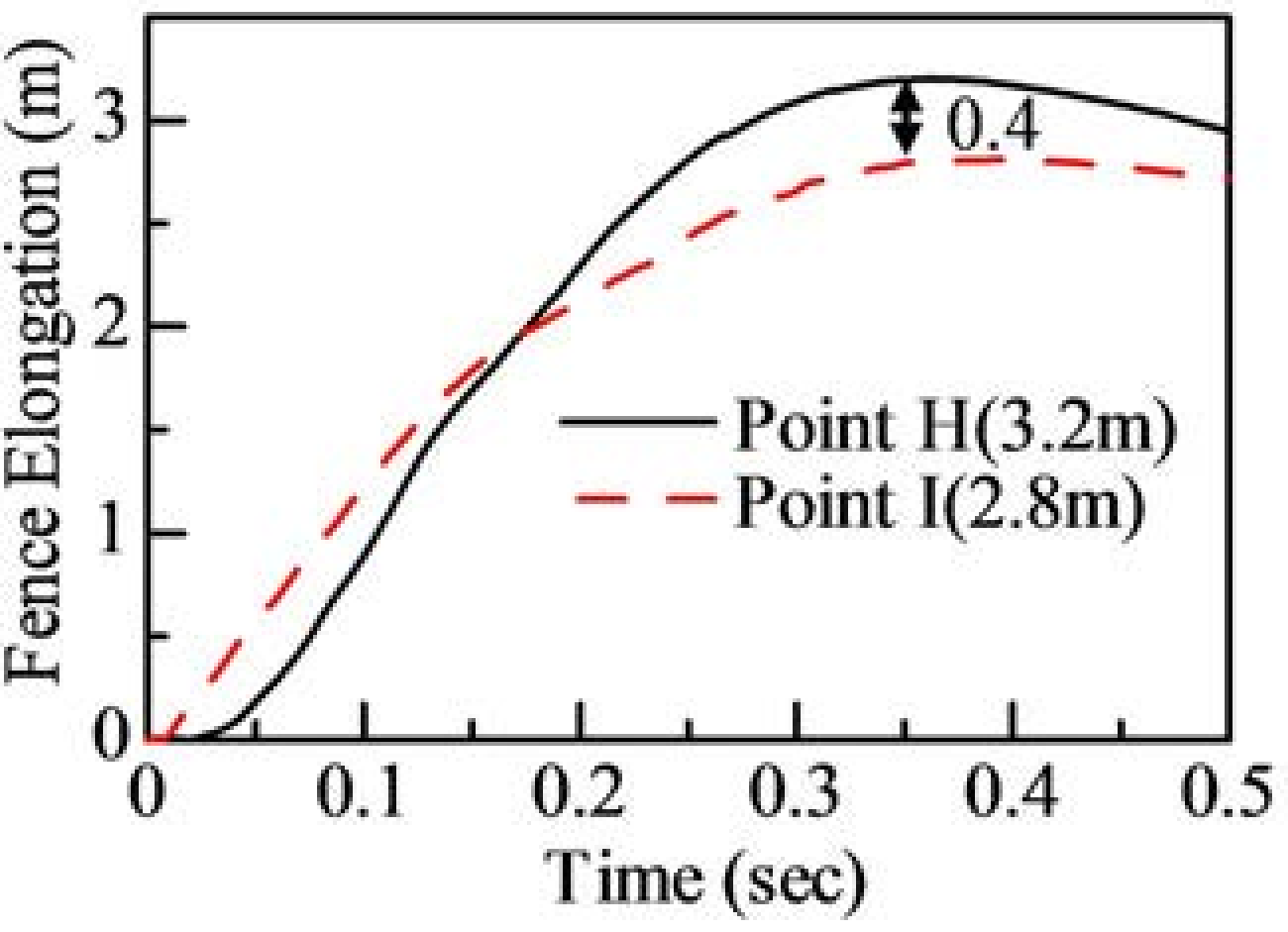
Fence Elongation (m)
3
2
1
0
0.4
Point H(3.2m)
Point I(2.8m)
0
0.1
0.2
0.3
0.4
0.5
Time (sec)

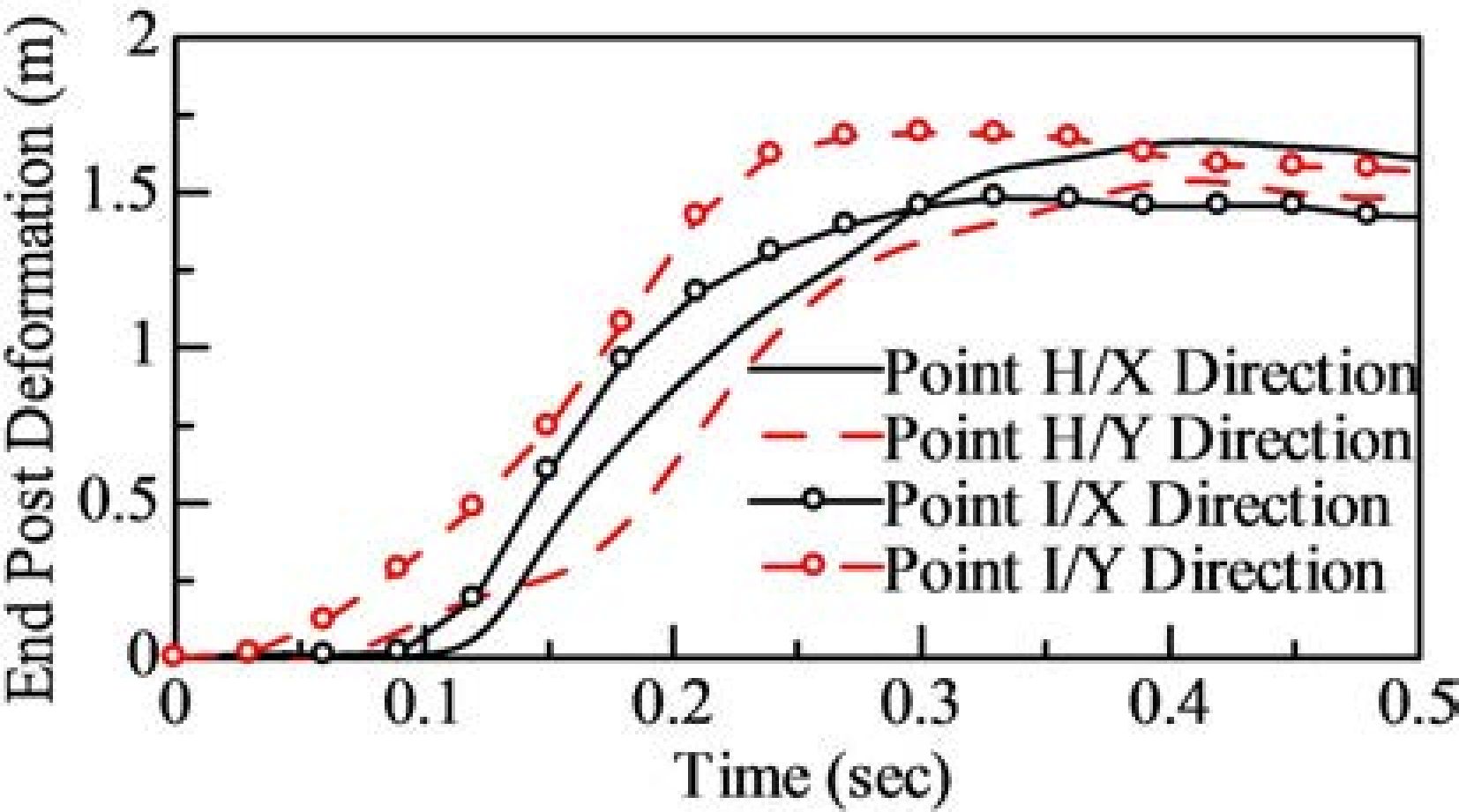
End Post Deformation (m)
2
1.5
1
0.5
0
0
0.1
0.2
0.3
0.4
0.5
Time (sec)
Point H/X Direction
Point H/Y Direction
Point I/X Direction
Point I/Y Direction

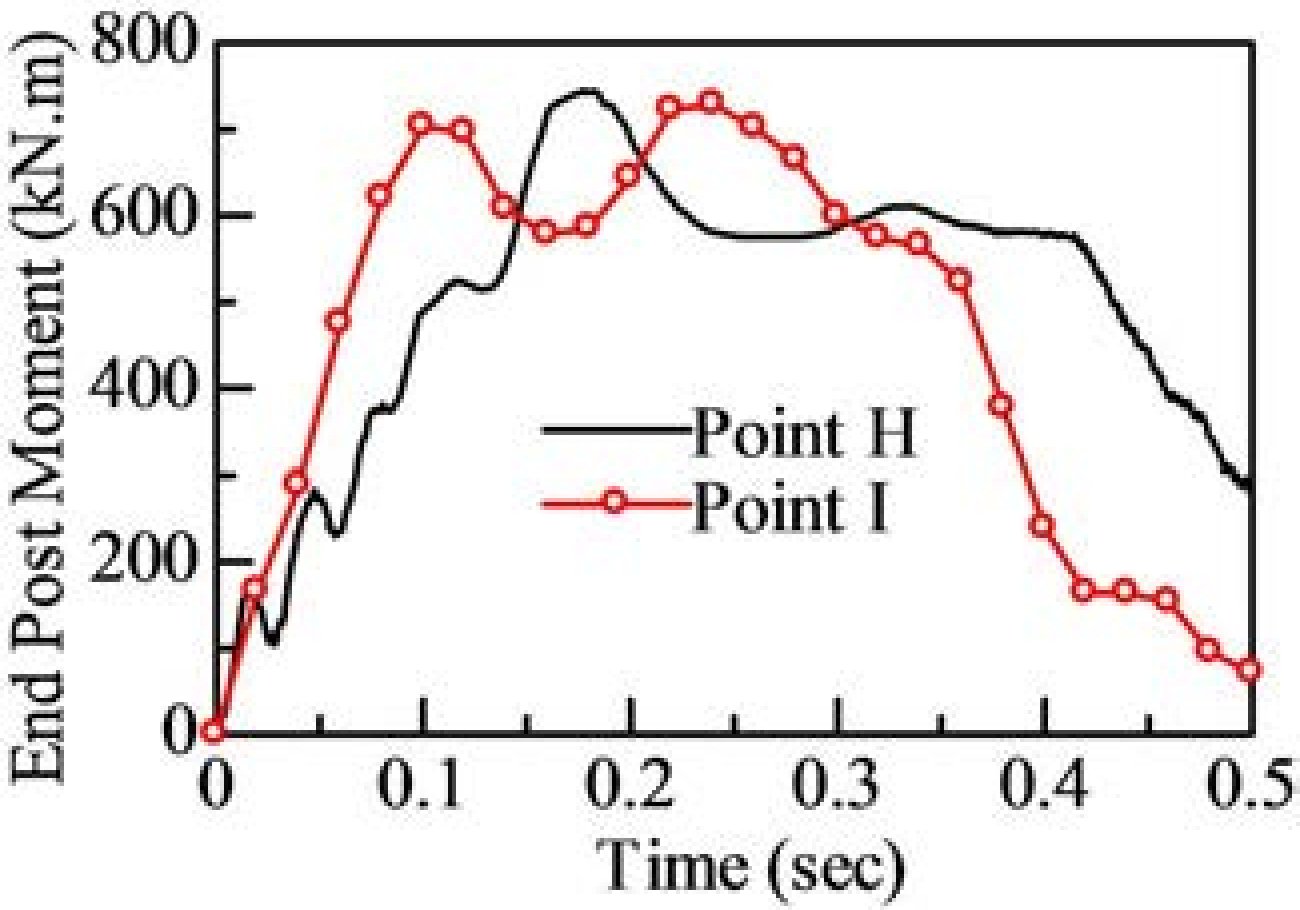
End Post Moment (kN.m)
800
600
400
200
0
0
0.1
0.2
0.3
0.4
0.5
Time (sec)
Point H
Point I

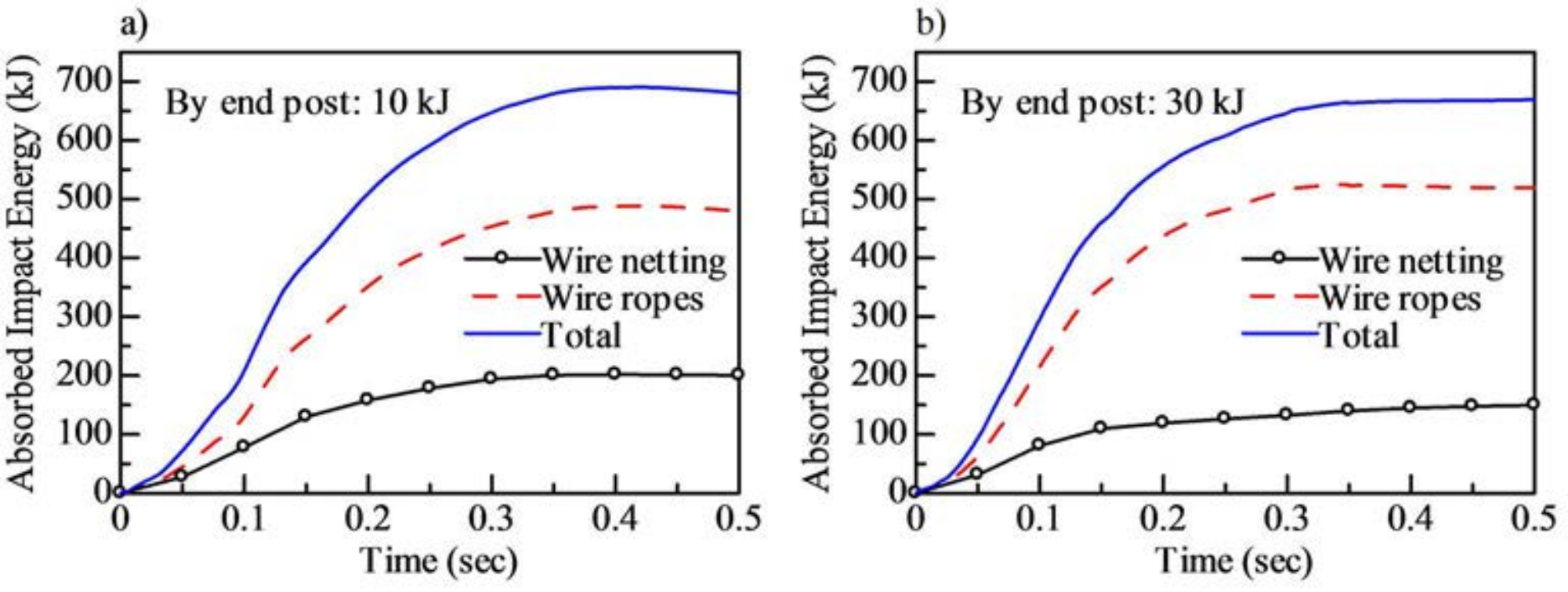
a)
By end post: 10 kJ
Absorbed Impact Energy (kJ)
Time (sec)
Wire netting
Wire ropes
Total
b)
By end post: 30 kJ
Absorbed Impact Energy (kJ)
Time (sec)
Wire netting
Wire ropes
Total

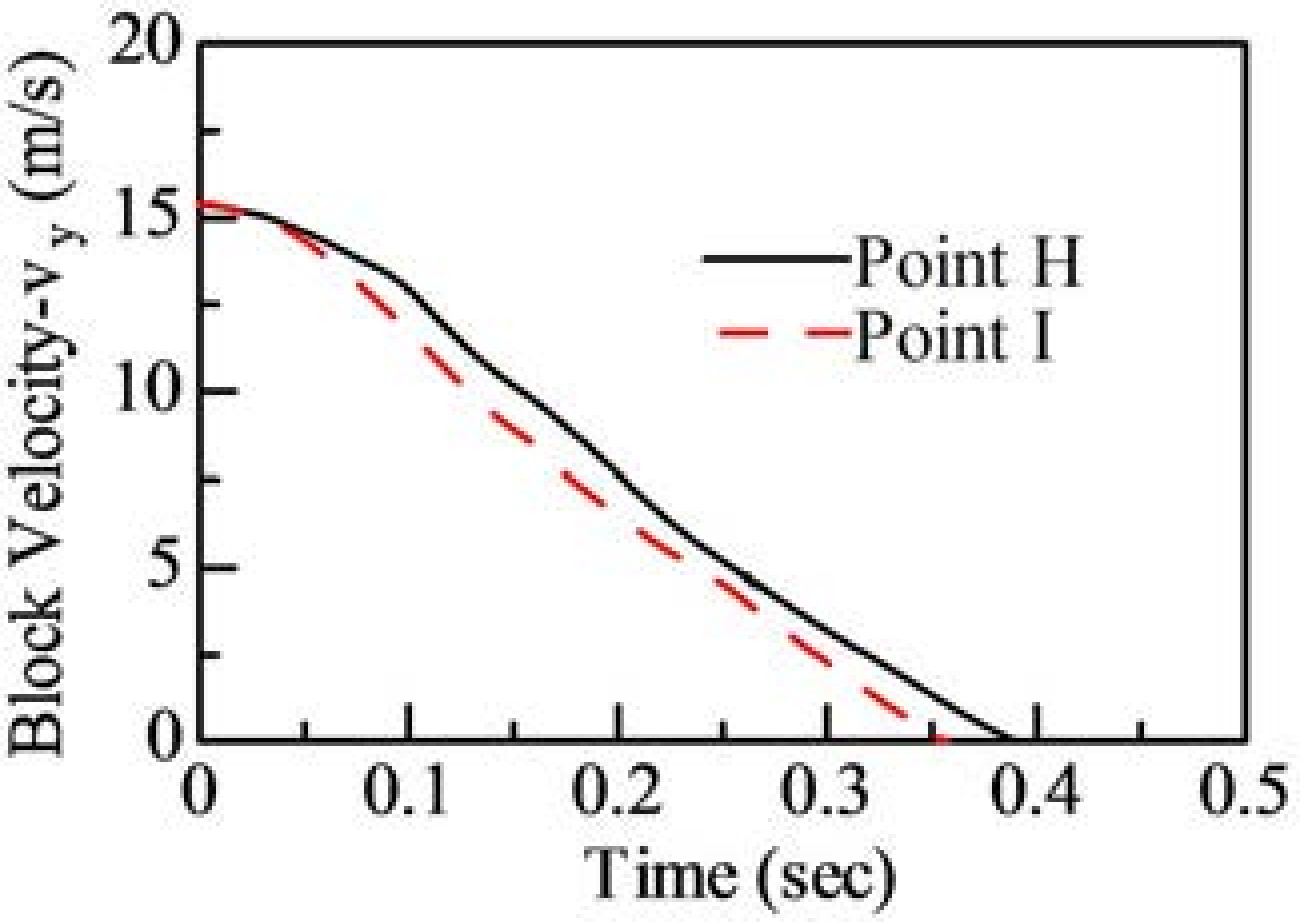
Block Velocity-v_y (m/s)
20
15
10
5
0
0
0.1
0.2
0.3
0.4
0.5
Time (sec)
Point H
Point I

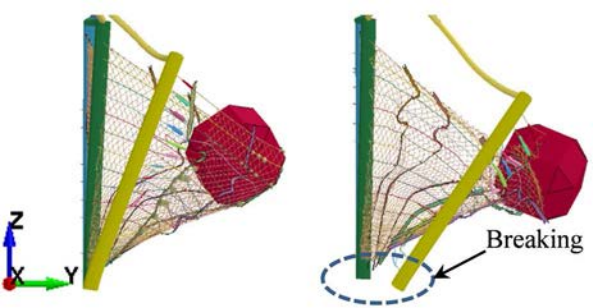
Z
X
Y
Breaking

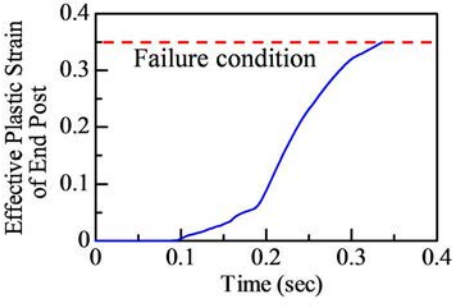
Failure condition
Effective Plastic Strain of End Post
0.4
0.3
0.2
0.1
0
0
0.1
0.2
0.3
0.4
Time (sec)

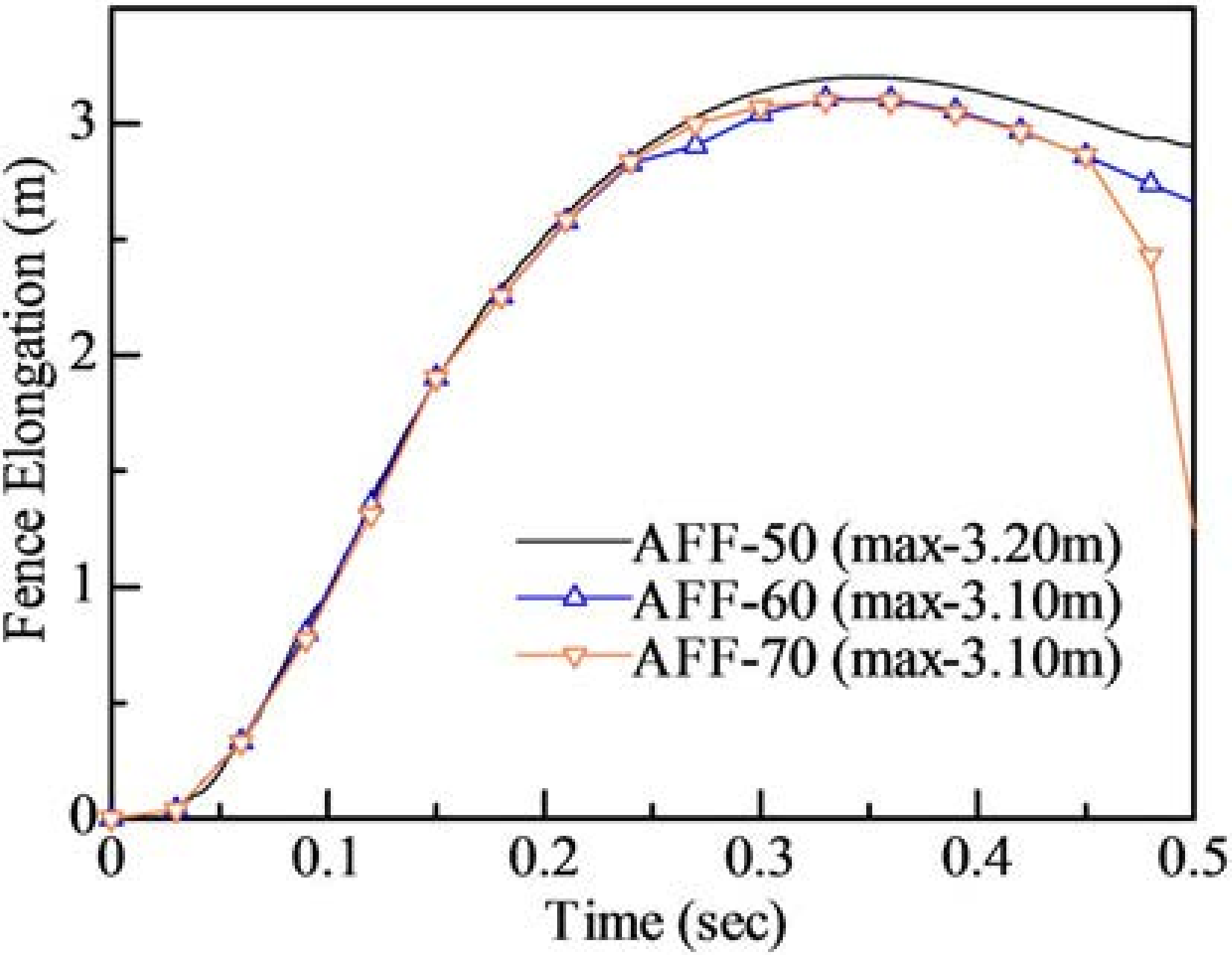
Fence Elongation (m)
0
1
2
3
0
0.1
0.2
0.3
0.4
0.5
Time (sec)
AFF-50 (max-3.20m)
AFF-60 (max-3.10m)
AFF-70 (max-3.10m)

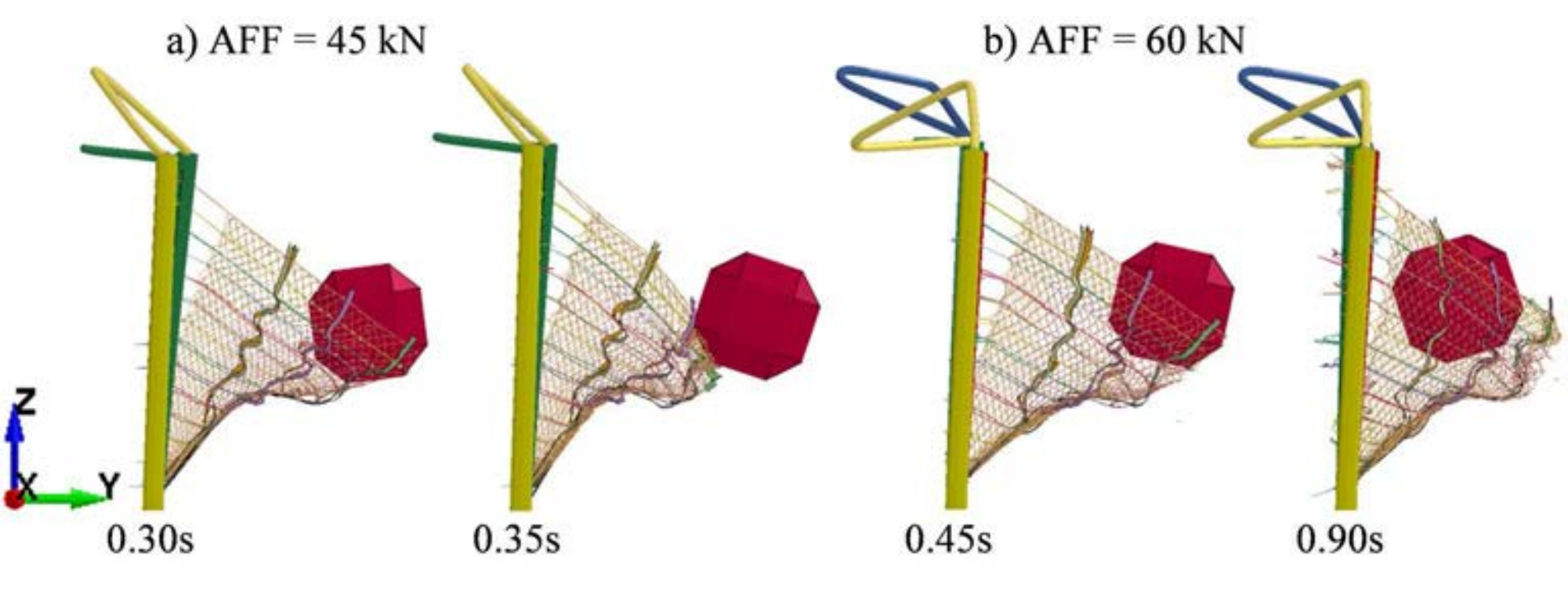
a) AFF = 45 kN
b) AFF = 60 kN
Z
X
Y
0.30s
0.35s
0.45s
0.90s

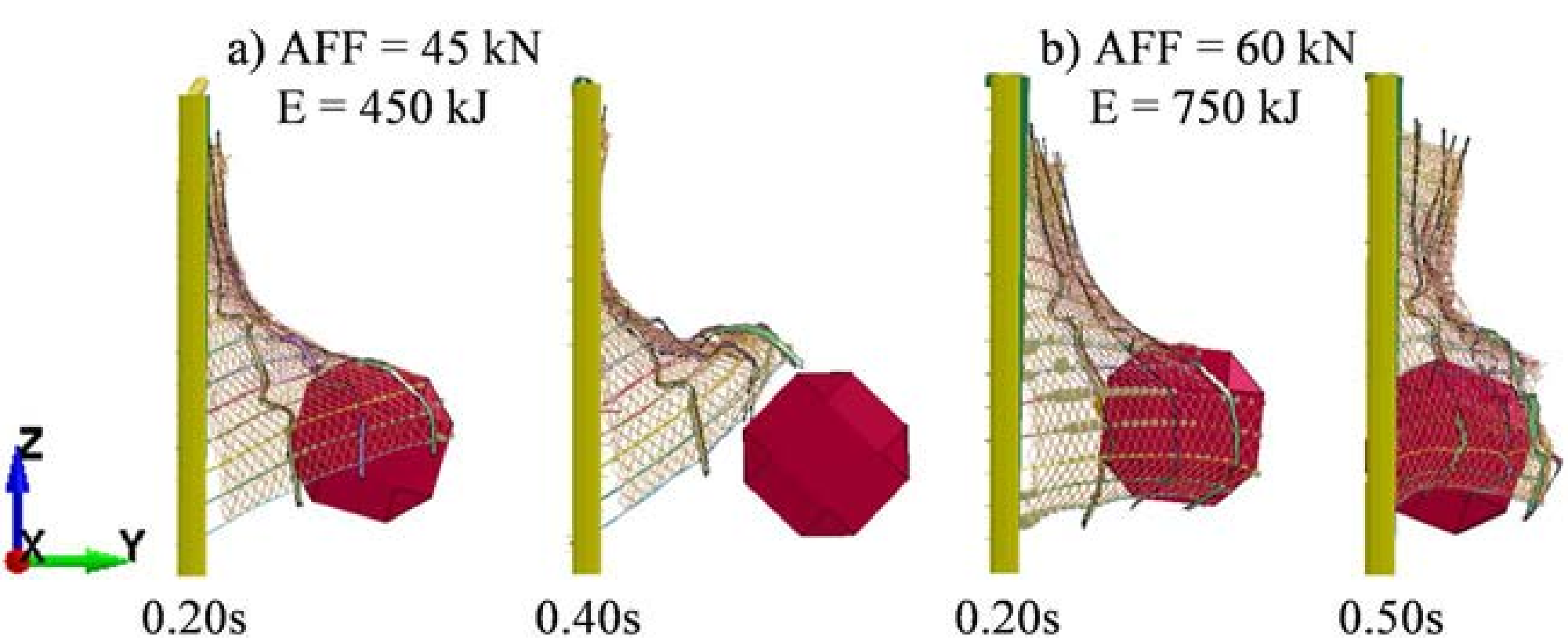
a) AFF = 45 kN
E = 450 kJ
b) AFF = 60 kN
E = 750 kJ
Z
X
Y
0.20s
0.40s
0.20s
0.50s

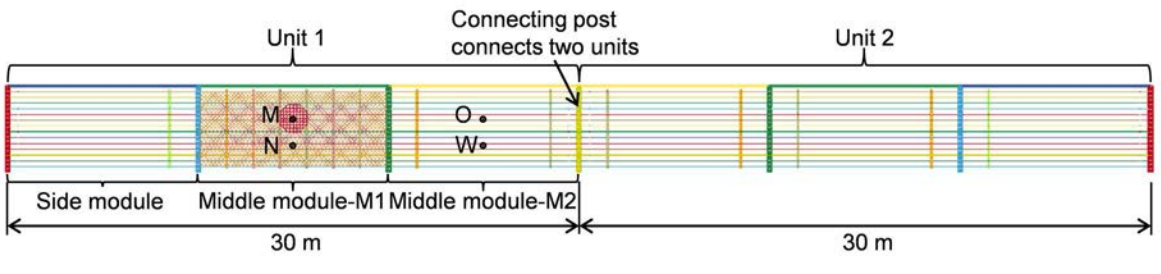
Unit 1
Connecting post
connects two units
Unit 2
M
N
O
W
Side module
Middle module-M1
Middle module-M2
30 m
30 m

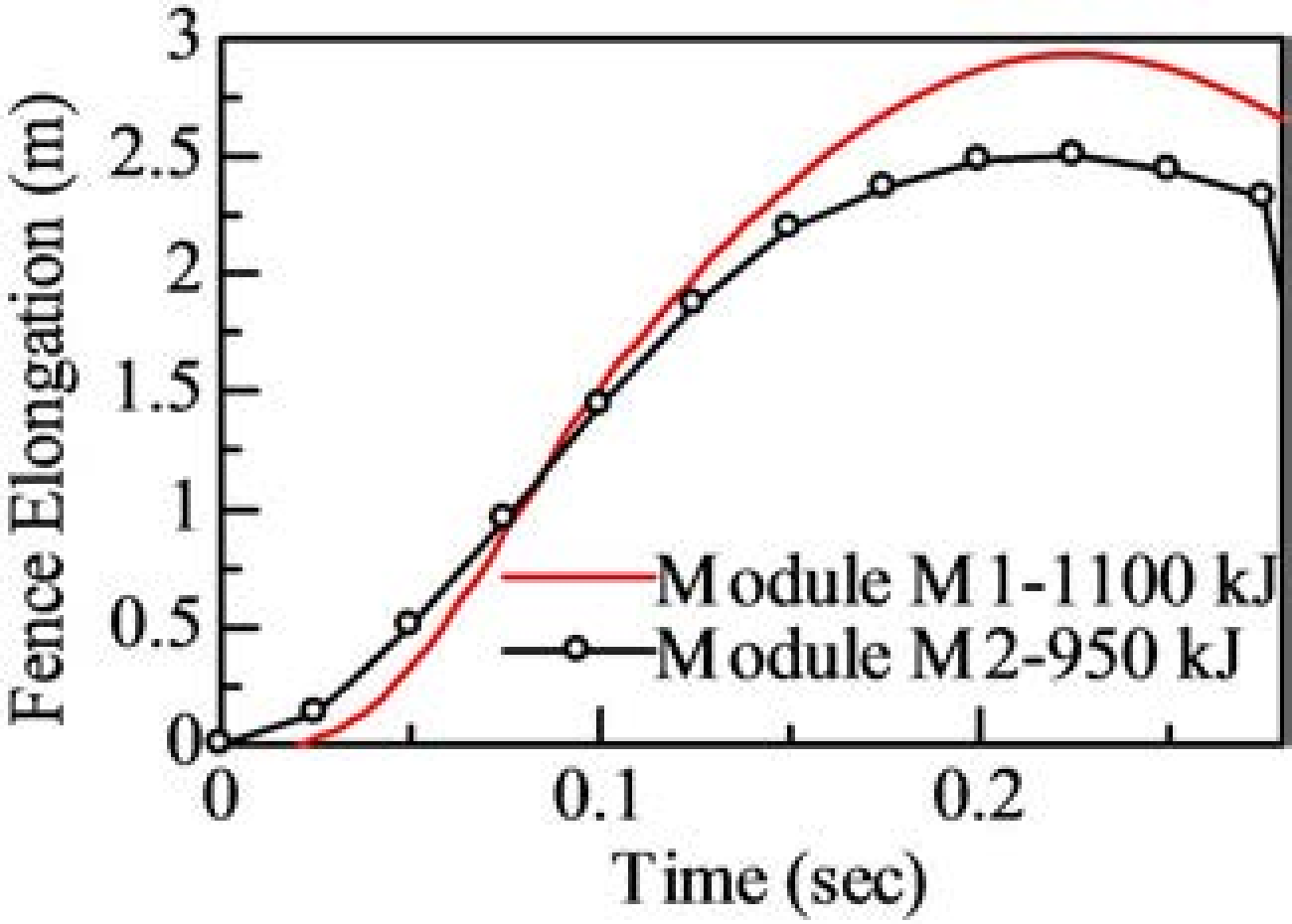
Fence Elongation (m)
3
2.5
2
1.5
1
0.5
0
0
0.1
0.2
Time (sec)
Module M1-1100 kJ
Module M2-950 kJ